The subcellular localization of myosin XVI in U2OS cells and its expression in the mouse brain

Master's Thesis

University of Turku

MSc Degree Programme in Biomedical Sciences

Drug Discovery and Development

May 2021

Jutta Joukio

Jolanta Lundgren (PhD), Rimante Minkeviciene (PhD), Prof. Ullamari Pesonen (PhD)

Institute of Biomedicine

The originality of this thesis has been checked in accordance with the University of Turku quality assurance system using the Turnitin Originality Check service.

UNIVERSITY OF TURKU
Institute of Biomedicine, Faculty of Medicine

JOUKIO, JUTTA: The subcellular localization of myosin XVI in U2OS cells and its expression in the mouse brain
Master's Thesis, 63 p
MSc Degree Programme in Biomedical Sciences/Drug Discovery and Development
May 2021

Myosin XVI is a neuronally expressed member of the myosin superfamily. Many aspects of this myosin remain mysterious, but its ability to regulate actin branching and indications of its enhanced expression in early development indicate a role in brain development. Intriguingly, the gene encoding myosin XVI has been linked to autism spectrum disorder and schizophrenia which both display disrupted neurodevelopment. Both are complex, debilitating and currently incurable conditions that have partly overlapping symptoms, including olfactory abnormalities that have recently attracted more interest.

This Master's Thesis investigated the subcellular localization and developmental expression of myosin XVI to enlighten its role in the brain. Localization pattern and interaction with filamentous actin were studied in human osteosarcoma cells by staining. The expression pattern was examined in the postnatal mouse olfactory bulb, hippocampus, cerebellum, and cortex by western blotting. The results suggest a principal localization to the perinuclear region where myosin XVI may regulate vesicle traffic. Myosin XVI was also observed to co-localize with actin on the cell membrane where it may regulate membrane protrusion. Additionally, findings indicate a role in cell division. Western blotting revealed a higher expression in early postnatal development compared to later stages, apart from the olfactory bulb where the expression remained more stable.

These observations support the hypothesis that myosin XVI can regulate neurodevelopment. Future research will need to clarify the molecular mechanisms and cellular distribution of myosin XVI in the brain, especially in the olfactory bulb. This can add to understanding of autism spectrum disorder and schizophrenia and, ultimately, enable better treatments.

Keywords: myosin XVI, autism spectrum disorder, schizophrenia, neurodevelopment

Table of contents

1 Introduction

1.1 Myosins and actin

Myosins are eukaryotic proteins that constitute a large and versatile superfamily of at least around 20 distinct myosin classes, likely many more (Foth et al., 2006; Sebé-Pedrós et al., 2014). These classes can further be divided into different subclasses (Sebé-Pedrós et al., 2014). Myosin classes are typically denoted by Roman numerals. Myosin class II was discovered first and myosins from this family thus referred to as conventional, whereas members of the other classes are designated as unconventional (Sellers, 2000).

Myosins come in many different forms, but they all share a motor, also known as head, domain at the N-terminus, a neck domain in the middle, and a tail domain at the C-terminus of their heavy chains (Foth et al., 2006; Hartman and Spudich, 2012). The head domain is highly conserved across different myosins and is the domain responsible for the famous motor function of myosins; it contains binding sites for adenosine triphosphate (ATP) and actin, and functions as a mechanoenzyme, or ATPase, that converts the chemical energy of ATP into mechanical force by hydrolysis (Hartman and Spudich, 2012; Sellers, 2000). The conformational changes in the ATP-binding site enable cyclic interactions between the myosin and actin (Hartman and Spudich, 2012). The neck domain can interact with myosin light chains and likely serves as a regulatory region (Foth et al., 2006). The tail domain, in turn, varies greatly between different myosin classes and is thought to be the major domain responsible for the diverse functions myosins play in cells (Foth et al., 2006; Hartman and Spudich, 2012). The tail domain may contain different functional motifs and typically binds adaptor proteins and other cellular binding partners that myosins interact with (Hartman and Spudich, 2012; Sellers, 2000).

As a consequence of their ability to interact with actin and to bind various other cellular molecules, myosins are known to be important for a wide repertoire of cellular processes (Hartman and Spudich, 2012; Krendel and Mooseker, 2005). Actin is a protein that is arranged into filaments that constitute the actin cytoskeleton of the cell (Carlsson, 2010). The actin cytoskeleton is a dynamic structure that undergoes continuous cycles of nucleation of new actin filaments from actin monomers, elongation of actin filaments by polymerization to produce filamentous actin (F-actin), and filament severing and depolymerization (Carlsson, 2010). F-actin is found principally in the cytoplasm, where it is organized into different linear and cross-linked meshworks (Svitkina, 2018). The dynamic

reorganization allows the actin cytoskeleton to provide support to the cell and act as an intracellular transportation network (Carlsson, 2010). Myosins are known to regulate many actin-related activities in the cell, including cell migration, cell adhesion, cytokinesis, intracellular transport, organelle anchoring, and membrane trafficking (de Lanerolle, 2012; Hartman and Spudich, 2012; Krendel and Mooseker, 2005).

1.2 Myosin XVI

1.2.1 Structure

The unconventional myosin class XVI (MYO16, also known as KIAA0865 and NYAP3) is a relatively recently found member of the myosin superfamily. It was initially screened from human by Nagase and colleagues in 1998, but the first systematic characterization of this myosin class was conducted by Patel and colleagues in 2001 (Nagase et al., 1998; Patel et al., 2001). Myosin XVI is only found in vertebrates and is likely specific to mammalian species, including human, which indicates that it developed rather late in the course of myosin evolution (Krendel and Mooseker, 2005; Thompson and Langford, 2002).

Patel et al. (2001) identified two myosin XVI subclasses, or isoforms, in rat (**Figure 1**). One isoform comprised a heavy chain of 1912 amino acids and the other a heavy chain of 1322 amino acids. These two isoforms appeared to display unique structural features in both the N-terminal and C-terminal domains. First, they have an extension at the N-terminus prior to the motor domain. This pre-motor domain contains a conserved myosin phosphatase N-terminal element, a protein phosphatase type 1 catalytic subunit-binding motif, and several ankyrin repeats (Patel et al., 2001; Telek et al., 2020). In addition, the pre-motor domain possesses a nuclear export signal (NES) sequence (Cameron et al., 2007). The pre-motor domain is followed by a motor domain that is highly similar to motor domains of other myosins, containing ATP- and actin-binding motifs (Patel et al., 2001). Next comes a short neck domain that contains one calmodulin-binding motif (Patel et al., 2001; Telek et al., 2020). After that begins the C-terminal tail domain, which also distinguishes the two isoforms as it is truncated in the shorter one (Patel et al., 2001). In the longer isoform, the tail domain includes a Wiskott–Aldrich syndrome protein/verprolin homologue 1 (WAVE1)-interacting region, and a neuronal tyrosine-phosphorylated adaptor for phosphoinositide 3-kinase (NYAP) homology motif (NHM) containing a nuclear localization signal (NLS) sequence and tyrosine residues, as well as a proline-rich region (Cameron et al., 2007; Patel et al., 2001; Telek et al., 2020).

The precise tertiary as well as potential quaternary structure of myosin XVI remains ambiguous as X-ray crystallography has not been performed. It is however likely that the two myosins of class XVI exist as monomers, because they appear to be most closely related to monomeric myosin class III members and because the tail domain does not contain motifs typically required for protein dimerization (Cameron et al., 2007; Patel et al., 2001).

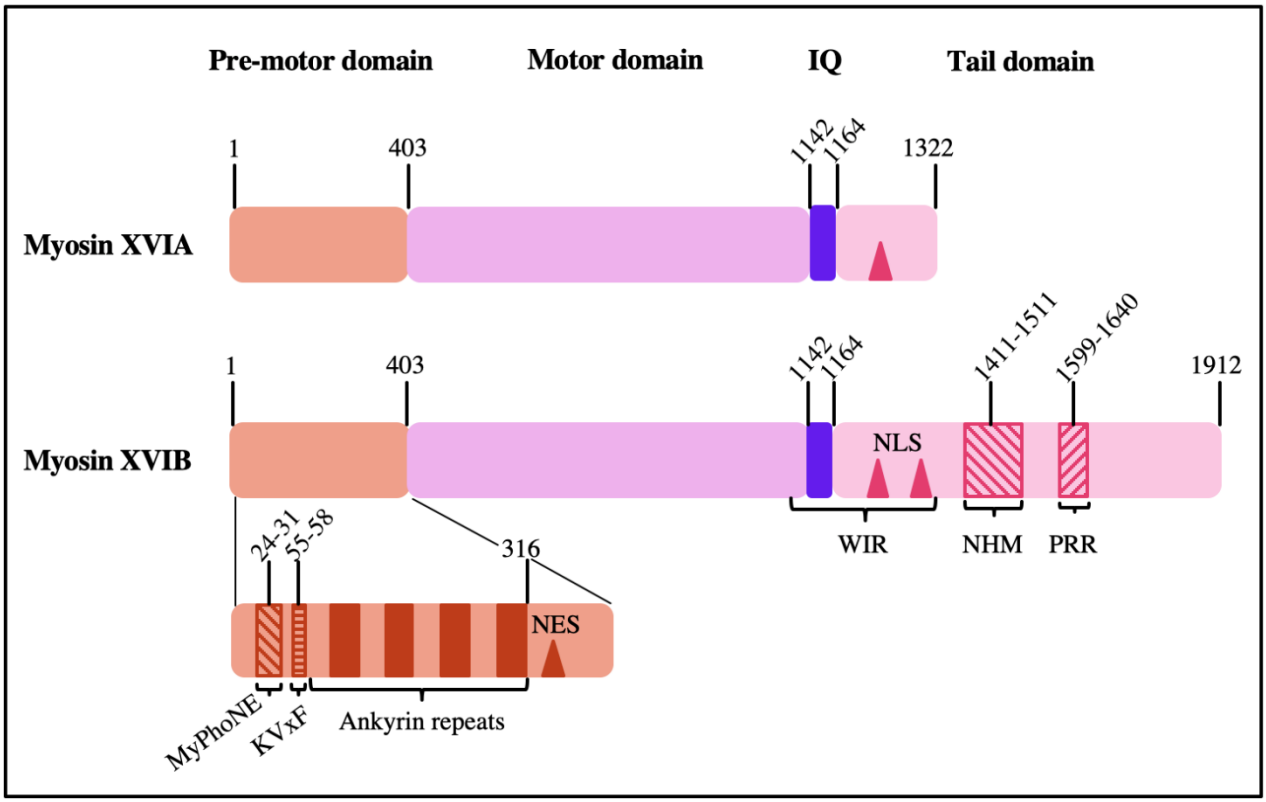

Figure 1. A schematic representation of the structure of myosin XVI isoforms A and B (adapted from Bugyi and Kengyel, 2020, and Telek et al., 2020). The amino acids are numbered and correspond to the rat isoforms. MyPhoNE, myosin phosphatase N-terminal element. KVxF, protein phosphatase type 1 catalytic subunit-binding motif. NES, nuclear export signal. IQ, calmodulin-binding motif. WIR, WAVE1-interacting region. NLS, nuclear localization signal. NHM, NYAP homology motif. PRR, proline-rich region.

The UniProtKB/Swiss-Prot database proposes four myosin XVI splice variants in human (NCBI RefSeq: NP_055826.1). The longest one, encoding for a heavy chain of 1858 amino acids, likely corresponds to the rat 1912 amino acid isoform with longer tail domain, based on sequence analyses (Patel et a., 2001; UniProtKB/Swiss-Prot). As for mouse, the UniProtKB/Swiss-Prot database describes three potential myosin XVI splice variants (NCBI RefSeq: NP_001306080.1), and the two longest ones, constituting 1919 amino acids, also likely correspond to the rat 1912 amino acid isoform. The deducted molecular masses for the long-tail myosin XVI isoforms in human, rat, and mouse are around 206 kDa, 211 kDa, and 213 kDa, respectively.

From now on, myosin XVI is used as a principal term when describing the protein in general. MYO16 (gene name *MYO16*) is used when discussing specifically the human form, whereas Myo16 (gene name *Myo16*) is used when discussing specifically the mouse or rat form. Likewise, the short-tail isoform myosin is designated as XVIA, MYO16A, or Myo16a, and the long-tail isoform as myosin XVIB, MYO16B, or Myo16b.

1.2.2 Cellular and subcellular distribution

Myosin XVI is expressed in many tissues, but its expression is enhanced in the central nervous system (Patel et al, 2001; The Human Protein Atlas). In rat, Myo16b is the principal isoform both in the brain and in the periphery, and Myo16a is expressed in considerably smaller quantities (Patel et al., 2001). Myosin XVI does not display prominent regional differences in the brain, but the expression level may be related to the developmental stage (Patel et al., 2001; The Human Protein Atlas). The expression of myosin XVI has mostly been studied in the rodent brain, especially in the cerebral cortex and cerebellum, but expression has also been detected widely in the human brain where MYO16 is found in the cerebral cortex, cerebellum, the limbic system including structures such as the hippocampus, olfactory region, and amygdala, and in many other regions (Patel et a., 2001; Roesler et al., 2019; The Human Protein Atlas; Yokoyama et a., 2011).

Myosin XVI is an intracellular protein. In primary rat astrocytes, cerebellar granule neurons, and hippocampal neurons, it localizes throughout the cytoplasm in a punctate manner, and occasionally to the intracellular surface of plasma membrane and around the nucleus (Patel et al., 2001). In mouse cerebellar Purkinje cells, Myo16 localizes to dendritic spines (Roesler et al., 2019). In the human fibroblast-like COS-7 cell line, MYO16 shows variable locations, including the cytoplasm and the nucleus (Cameron et al., 2007). Inside the nucleus, it appears to localize diffusely in the nucleoplasm, excluding the nucleoli (Cameron et al., 2007; Cameron et al., 2013). MYO16 has also been described in vesicles in the neuronal SH-SY5Y cell line (The Human Protein Atlas). Previous results indicate that the myosin XVIA isoform is cytoplasmic but the B isoform is both cytoplasmic and nuclear (Bugyi and Kengyel, 2020; Cameron et al., 2013). The localization might be dependent on the phase of the cell cycle, which would explain the variable locations (Cameron et al., 2013).

1.2.3 Molecular interactions and proposed biological functions

The KVxF motif in the pre-motor domain of myosin XVI corresponds to the consensus protein phosphatase type 1 catalytic subunit (PP1c) sequence identified in many PP1c-binding proteins (Patel

et al., 2001). Myosin XVI is therefore assumed to interact with PP1c and control dephosphorylation of intracellular proteins (Kengyel et al., 2015; Patel et al., 2001). Considering the ability of PP1c to regulate a broad range of cellular functions, it is likely that the pre-motor domain of myosin XVI has important roles in contributing to its functions (Cohen, 2002; Kengyel et al., 2015). However, the specific outcomes of the interaction with PP1c are not yet known. Ankyrin repeats are commonly known to mediate protein–protein interactions, which indicates that the pre-motor domain of myosin XVI may contribute to the function through various other intermolecular interactions as well (Mosavi et al., 2004). In addition, the pre-motor domain may also modulate intramolecular interactions, such as the ATPase activity of the motor domain (Kengyel et al., 2015).

The motor domain of myosin XVI co-sediments with F-actin in an ATP-sensitive manner and is therefore assumed to function as an ATPase as most other myosins (Patel et al., 2001). This function has not been established, however, and more recent sequence analyses propose that myosin XVI may have a reduced ATPase activity (Cameron et al., 2007).

The long tail domain of myosin XVIB has attracted special interest as it is considered to mediate the major cellular function of the protein. The NHM motif in the tail domain contains tyrosine residues that can be phosphorylated by a protein-tyrosine kinase FYN, induced by Contactin (Yokoyama et al., 2011) (**Figure 2**). Presumably mediated by this phosphorylation, myosin XVIB can interact with the p85 subunit of phosphoinositide 3-kinase (PI3K) (Yokoyama et al., 2011). This leads to activation of the downstream effector proteins of the PI3K pathway, such as RAC1, which in turn triggers the activation of the WAVE1 subunit of the WAVE regulatory complex (WRC) (Yokoyama et al., 2011). Myosin XVIB can also directly interact with components of the WRC, through the region located prior to the NHM motif in the protein sequence (Yokoyama et al., 2011). The activated WRC further stimulates the actin-related protein 2/3 (Arp2/3) complex that is responsible for nucleation of branched actin filaments (Goley and Welch, 2006; Takenawa and Suetsugu, 2007). Hence, myosin XVIB isoform likely regulates reorganization of the actin cytoskeleton by activating the PI3K–WRC–Arp2/3 pathway and by recruiting the WRC near to PI3K to facilitate the conversion of signals into action. Additionally, the proline-rich region in the tail domain of myosin XVIB possibly comprises binding sites for profilin and ENA/VASP homology proteins, suggesting that it also interacts with these regulators of actin polymerization (Patel et al., 2001; Prehoda et al., 1999). For instance, ENA/VASP proteins are associated with actin-dependent cell motility are required for targeting the actin polymerization machinery to sites of cytoskeletal remodeling where they affect the function of the Arp2/3 complex (Krause et al., 2003; Prehoda et al., 1999).

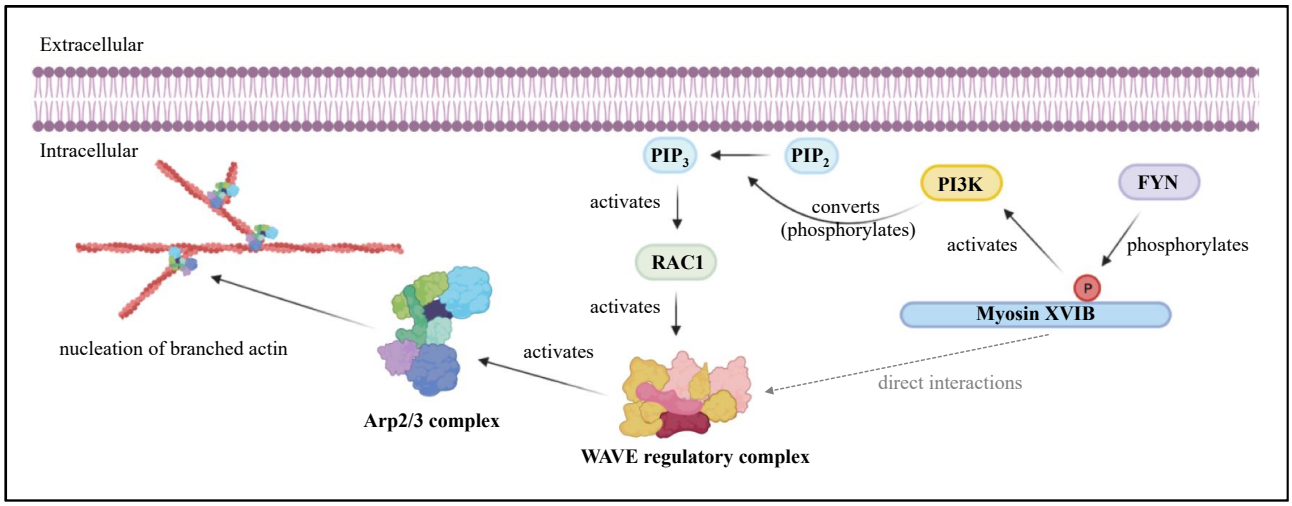

Figure 2. A simplified illustration of the proposed intracellular signaling pathway of myosin XVIB in the regulation of the branched actin formation (adapted from Telek et al., 2020). Tyrosine residues (P) in the tail domain of myosin XVIB are phosphorylated by FYN, which triggers activation of phosphoinositide 3-kinase (PI3K). PI3K converts phosphatidylinositol 4,5-bisphosphate (PIP_2) to phosphatidylinositol (3,4,5)-trisphosphate (PIP_3) on the plasma membrane. PIP_3 in turn activates downstream signaling molecules, such as RAC1 that further activates the WAVE regulatory complex. The WAVE regulatory complex stimulates Arp2/3 complex that is responsible for nucleation of branched actin filaments. Myosin XVIB may also have direct interactions with the WAVE regulatory complex through the WAVE1-interacting region of the tail domain.

Arp2/3 complex activity and branched actin formation are important for many cellular events. These include 1) organization of lamellipodial protrusions at the leading edge of the cell during migration, 2) organization of adhesion sites, 3) intracellular vesicle transport, and 4) endocytosis and exocytosis, for example (Goley and Welch, 2006) (**Figure 3**).

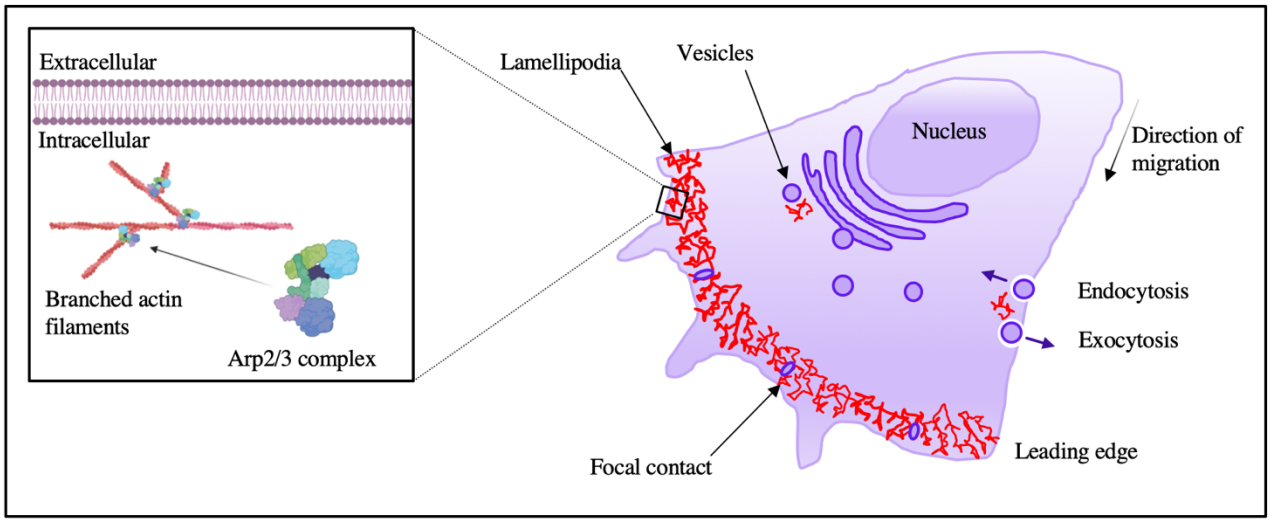

Figure 3. An illustration of some locations of the Arp2/3 complex and branched actin filaments (red) in the cell (adapted from Goley and Welch, 2006). Branched actin is found in lamellipodia which are located linearly to the leading edge of the cell. Branched actin is also found at focal contact sites. In addition, branched actin formation is required for intracellular vesicle traffic, endocytosis, and exocytosis.

Since myosin XVI is highly expressed in the brain, earlier studies have aimed to elucidate its role there. Previous studies suggest that myosin XVI expression depends on the developmental stage, being highest shortly after birth, and also that myosin XVI is most active during the period of pre- and neonatal brain development (Patel et al., 2001; Yokoyama et al., 2011). More specifically, myosin XVI may regulate neurite outgrowth and regulation of dendritic spines and synapses in the developing brain. These are discussed next.

Neurite outgrowth refers to the growth of dendrites and axons from the neuronal cell body (Sainath and Gallo, 2015). Myosin XVI is supposed to regulate neurite elongation and also neuronal morphogenesis through its actions on PI3K signaling, triggering not only the PI3K–WRC–Arp2/3 pathway but possibly other parallel pathways as well (Yokoyama et al., 2011). Two types of actin-rich projections are found at the leading edge of the elongating neurites; filopodia and lamellipodia (Sainath and Gallo, 2015). Arp2/3 complex activity and actin branching is frequently ongoing in lamellipodia (Goley and Welch, 2006). Therefore, it is possible that myosin XVI operates there.

Synaptic function largely depends on the structure and disposition of dendritic spines (Hotulainen and Hoogenraad, 2010). Dendritic spines are small protrusions that bulge from the main shaft of dendrites and are found postsynaptically at most excitatory synapses (Bourne and Harris, 2008; Hering and Sheng, 2001; Hotulainen and Hoogenraad, 2010). Dendritic spines are enriched with branched actin (Hotulainen and Hoogenraad, 2010). They are typically found in both excitatory and inhibitory neurons, however several classes of neurons also lack dendritic spines, such as many inhibitory interneurons (Hering and Sheng, 2001; Scheuss and Bonhoeffer, 2014). Changes in the size, shape, and distribution of dendritic spines are thought to serve as the molecular basis for synaptic plasticity, and the spines are considered as the major sites for information processing and storing in the brain (Hering and Sheng, 2001; Hotulainen and Hoogenraad, 2010). For example, alterations in the structure and function of the spines in hippocampal neurons are among the key determinants of neural processes underlying learning and memory (Bourne and Harris, 2008).

Logically, then, disturbances in the PI3K–WRC–Arp2/3 pathway can jeopardize the function of dendritic spines and thereby neuronal plasticity. For example, hippocampal neurons from *Wave1* knockout mice have abnormal neuronal morphology, growth cone dynamics, and dendritic development, density, and receptor composition (Soderling et al., 2007). Similarly, hippocampal neurons from *Arp2/3 subunit* knockout mice show functionally immature synapses and structurally deficient dendritic spines (Hotulainen et al., 2009; Spence et al., 2016). Myosin XVI, a regulator of both WRC and Arp2/3 as discussed above, has also been found in dendritic spines in cerebellar

Purkinje cells in mice (Roesler et al., 2019). In *Myo16* knockout mice, actin turnover is accelerated in the dendritic spines of Purkinje cells, indicating that depletion of myosin XVI may result in a faster actin turnover rate (Roesler et al., 2019). However, the density of dendritic spines remains unaltered in Purkinje cells lacking myosin XVI as compared to cells where the protein is normally expressed (Roesler et al., 2019). In addition to its proposed postsynaptic functions, myosin XVI also appears to be important for presynaptic structure as well as for the number of synaptic vesicles (Roesler et al., 2019). Myosin XVI may also participate in cell adhesion at synapses. Some findings indicate that it interacts with neurexin 1-α (NRXN1α), a pre-synaptic membrane cell adhesion molecule, and with Kin of IRRE-like protein 3 (KIRREL3), another synaptic protein that participates in cell adhesion (Liu et al., 2015; Nakayama et al., 2002).

Two more identified binding partners of myosin XVI are GTPase Regulator Associated with Focal Adhesion Kinase-1 (GRAF1) and Acyl-CoA thioesterase 9 (ACOT9) (Yokoyama et al., 2011). Interaction with GRAF1 suggests that myosin XVI may play a part in endocytic events, as GRAF1 regulates the clathrin-independent endocytic pathway (Lundmark et al., 2008). Interaction with ACOT9 suggests a role in intracellular fatty acid metabolism, since ACOT9 hydrolyzes Coenzyme A esters (Tillander et al., 2014).

Finally, myosin XVI may also participate in regulation of the cell cycle (Cameron et al., 2007; Cameron et al., 2013). The PI3K pathway is essential not only for Arp2/3-dependent formation of branched actin but also for various other cellular events, including neuronal survival and differentiation, supporting this hypothesis (Laurino et al., 2005; Rodgers and Theibert, 2002). Cameron et al. (2007, 2013) have found that the subcellular localization and expression level of myosin XVI may vary depending on the phase of the cell cycle. Expression of myosin XVI mRNA is highest during the interphase when the subcellular localization of the protein is restricted to the nucleus and is reduced during mitosis when the protein is dispersed outside the nucleus (Cameron et al., 2007; Cameron et al., 2013). Myosin XVI may regulate progression of the cell cycle, so that loss of myosin XVI can even lead to apoptosis (Cameron et al., 2013). The function in cell cycle regulation is supported by the NLS and NES sequences found in myosin XVI. The presence of these sequences implicates that myosin XVI may shuttle between the nucleus and cytoplasm; NLS tags a protein to be imported into the nucleus, whereas NES tags a protein to be exported out of there (Di Ventura and Kuhlman, 2016).

1.3 Myosin XVI and mental disorders

1.3.1 Autism spectrum disorder

Autism spectrum disorder (ASD) comprises a group of conditions that are manifested by a lack of social and emotional interaction and communication, stereotypic behaviors (e.g., repetitive movements), restricted interests, problems with speech and language, and often also cognitive, sensory, and motor abnormalities (Abrahams and Geschwind, 2008; Hodges et al., 2020; Vijayajumar and Judy, 2015). As the word 'spectrum' indicates, ASD is an umbrella term under which there are variable conditions ranging from mild to severe (Vijayajumar and Judy, 2015). Although each individual affected by ASD has a unique combination of symptoms, ASD is typically classified into four main categories, namely Asperger's syndrome, classical autistic disorder, childhood disintegrative disorder, and pervasive developmental disorder not otherwise specified (Vijayajumar and Judy, 2015). First symptoms of ASD typically emerge early in development, before the age of three years (Hodges et al., 2020). The prevalence of ASD is estimated to be around 1% globally, and it appears to be higher in males and in Caucasian populations (Hodges et al., 2020).

Sensory symptoms are a newer category included in the diagnostic criteria of ASD, as they have been increasingly recognized as one of the central symptoms (Hodges et al., 2020). It has been proposed that the sensory symptoms are not just secondary symptoms but instead directly grounded in the pathophysiological mechanisms of ASD, and even that the sensory abnormalities may lead to other behavioral impairments (Hazen et al., 2014). Sensory symptoms include sensory hyperreactivity, sensory hyporeactivity, and sensory-seeking behavior which refers to showing special interest in sensory information of the environment (Hazen et al., 2014; Hodges et al., 2020). Sensory stimuli can encompass any of the five senses, but abnormalities in smell, taste, and touch have been reported to be most common (Hazen et al., 2014). In terms of the sense of smell, several studies have found that detection and identification of olfactory stimuli is significantly worsened in autistic individuals compared to non-affected individuals (Bennetto et al., 2007; Sweigert et al., 2020). Sensory symptoms appear to be highly prevalent, as studies suggest that 55–70% of autistic people have these (Hazen et al., 2014).

Despite extensive research, the etiology of ASD remains elusive (Chen et al., 2015). High heritability, confirmed by twin and family studies, however points to strong contribution of genetic factors (Bailey et al., 1995; Folstein and Piven, 1991; Messinger et al., 2013). In addition to inherited mutations or variations, non-heritable *de novo* variants are also common (Chen et al., 2015). A large number of

genes contributing to ASD have been identified in many different studies, yet much of the genetic variation in ASD remains inexplicable (Manolio et al., 2009; Roberts et al., 2014; Wang et al., 2009). Although the genetic basis of ASD is now undisputed, environmental factors also play a part and are likely entangled with the genetic mechanisms (Vijayajumar and Judy, 2015). The current view on genetics is that in most cases ASD is caused by a combination of multiple genetic risk variants that each have only a small effect on the pathogenesis, rather than by a single gene (Cook and Scherer, 2008). This has complicated the elucidation of the etiology as ASD is a very heterogenous condition (Chen et al., 2015). It is likely that ASD comprises several different subphenotypes (Hu and Steinberg, 2009).

The well-established view is that ASD is a neurodevelopmental condition (Chen et al., 2015). But how exactly it affects the nervous system is not clear. An increased overall brain size during the early childhood is a typical finding in ASD, as well as abnormalities in the cytoarchitecture of the cerebral cortex, cerebellum, and parts of the limbic system such as the hippocampus and amygdala (Chen et al., 2105). Current models of ASD pathophysiology propose dysconnectivity of brain networks, neuroinflammation, growth dysregulation, abnormal synaptogenesis and synaptic dysfunction, altered serotonin activity, and altered signaling between neurons and glial cells, among other hypotheses (Chen et al., 2015; Kennedy and Adolphs, 2012; Samsam et al., 2014). Synaptic dysfunction is supported by mutations in synaptic proteins and findings of dendritic spine abnormalities, imbalances in excitatory/inhibitory neurotransmission, and a decreased number of inhibitory interneurons (Chen et al., 2015; Penzes et al., 2011; Zoghbi and Bear, 2012).

1.3.2 Schizophrenia

Schizophrenia is a neuropsychiatric disorder characterized by positive, negative, and cognitive symptoms (Millan et al., 2016). Positive symptoms – referring to experiences that are present when they should be absent – include psychotic behaviors, such as delusions and hallucinations (Millan et al., 2016). Negative symptoms – referring to experiences that are absent when they should be present – include flattened emotional expression and feelings, lack of pleasure and motivation, and decreased speech, for example (Millan et al., 2016). Cognitive symptoms include disorganized thinking and speech, and deficits in executive function (Millan et al., 2016). In addition, individuals with schizophrenia often exhibit impairments in motor and social function, such as social withdrawal, and sensory abnormalities (Millan et al., 2016). The typical onset of schizophrenia is during late adolescence or early adulthood (Forrest et al., 2018).

Sensory symptoms are common in schizophrenia, and they appear to extend beyond the visual and auditory hallucinations traditionally associated with it (Javitt, 2009). For example, olfaction is one of the sensory systems often affected (Javitt, 2009; Moberg et al., 2014). Schizophrenic individuals frequently exhibit substantial impairments in their ability to sense, identify, and discriminate odors (Moberg et al., 2014). An impaired sense of smell may even predict the development of psychosis (Moberg et al., 2014).

Like ASD, schizophrenia is an etiologically and symptomatically complex and chronic disorder that affects about 1% of the population worldwide (Millan et al., 2016). Many genetic, epigenetic, and environmental risk factors have been identified, but a comprehensive understanding of the pathogenesis remains unattained (Millan et al., 2016; Patel et al., 2014). Schizophrenia is also considered to be a result of disrupted neurodevelopment (Millan et al., 2016). Brain imaging findings point to structural and functional abnormalities in the cerebral cortex, hippocampal region, thalamus, and cerebellum, as well as in white matter tracts and ventricles (Andreasen and Pierson, 2008; Harrison, 1999; Millan et al., 2016; Van den Heuvel and Fornito, 2014). Plausible pathophysiological mechanisms include unbalanced glutamate and dopamine neurotransmission, aberrant neuronal connectivity, altered synaptic development and dendritic spines, and interneuron dysfunction (Marin, 2012; Moghaddam et al., 2012; Patel et al., 2014; Penzes et al., 2011; Pettersson-Yeo et al., 2011; Rapoport et al., 2012).

1.3.3 Links between *MYO16,* ASD, and schizophrenia

Genetic studies have found that *MYO16* is one of the genes linked to ASD. This is evident in genetic databases collecting results from many different ASD patient cohorts (DECIPHER, SFARI). One method to study the genetic risk factors is the genome-wide association studies that usually aim to identify single nucleotide polymorphisms (SNPs) in case–control cohorts (Connolly et al., 2013). Another common method, chromosomal microarray analysis, can detect copy number variants such as deletions and duplications (Roberts et al., 2014). A meta-analysis combining analyses from two large ASD cohort studies revealed eight SNPs, at the chromosomal locus 13q33.3 near the *MYO16* gene, that may be associated with ASD (Wang et al., 2009). Another study identified five SNPs with suggestive association to ASD in the intergenic region between *MYO16* and *IRS2* genes in males, but not in females, affected by ASD (Chang et al., 2013). This intergenic region is not presumed to contain any protein-coding genes, suggesting that although the *MYO16* gene itself may remain unaffected, the regulatory elements controlling its transcription can mediate harmful effects (Chang

et al., 2013). Three more studies found that some patients with ASD have deletions in *MYO16* (Friedman et al., 2009; Liu et al., 2015; Tucker et al., 2011).

Nevertheless, myosin XVI may affect the pathogenesis of ASD also indirectly. Many of the risk genes that predispose to ASD encode proteins that participate in regulation of neurite outgrowth, cell adhesion, synapse formation and maintenance, indicating that they act on common pathways in the cell (Joensuu et al., 2018; Liu et al., 2016). Assuming that myosin XVI is a crucial player in actin cytoskeleton remodeling and synapse regulation, disruptions in the function of other proteins working together with myosin XVI in these roles may result in altered function of myosin XVI as well. Suggestive to this possibility are the findings that myosin XVI may interact with some synaptic proteins, such as KIRREL3 and NRXN1, whose mutations have been linked to ASD (Gauthier et al., 2011; Liu et al., 2015; Nakayama et al., 2002)

MYO16 has also been linked to schizophrenia (Rodriguez-Murillo et al., 2014; SZDB). According to SZDB gene database, alterations in *MYO16* are usually intronic SNPs. One study employing exome sequencing of schizophrenic patients found that SNP in *MYO16* results in a loss-of-function mutation (Kenny et al., 2014).

1.3.4 Shared features of ASD and schizophrenia

ASD and schizophrenia may seem unrelated at first glance, but they share several features. First, both are intricate and heterogenous conditions with unclear root causes. A strong genetic basis and an interplay between genetic and environmental factors is evident in both. A large pool of genes that may contribute to the pathogeneses have been identified in both ASD and schizophrenia, and common genes and genetic loci have also been found (Kenny et al., 2014; Millan et al., 2016). One of the genes reported to be affected in both disorders is *MYO16*.

Second, both ASD and schizophrenia display aberrant neurodevelopment. The time of onset of the symptoms in these disorders, the early childhood in ASD and late adolescence or early adulthood in schizophrenia, also coincides with the period of vigorous brain development and maturation (Andersen, 2003). Key processes in brain development include cell differentiation, migration, neurite outgrowth, formation and pruning of synapses, and establishment of synaptic connections and neuronal networks (Andersen, 2003). In human, early childhood in particular is characterized by rapid neurite outgrowth, generation of glial cells, and establishment of synaptic connections, but remarkable structural and molecular reorganization of cells and synapses continues at least until

adolescence (Zhao and Bhattacharyya, 2018). ASD and schizophrenia may affect similar biological processes, including the regulation of synaptic function, neuronal connectivity, and interneurons. Abnormal dendritic spines are found in both disorders, and it has been hypothesized that the number of dendritic spines is higher than normal in autistic individuals and lower than normal in schizophrenic individuals (Penzes et al., 2011). On the other hand, some studies have indicated that the expression of MYO16 is lower than normal in the autistic brain and higher than normal in the schizophrenic brain (Liu et al., 2015; Rodriguez-Murillo et al., 2014). Aberrant regulation of dendritic spines could affect synapse formation, elimination, and maintenance, and further compromise the normal neurodevelopment (Penzes et al., 2011). In addition to these mechanisms, ASD and schizophrenia likely affect the same brain structures, such as the cerebral cortex, the limbic system, and the cerebellum.

Third, autistic and schizophrenic individuals display partly similar symptoms. These include social deficits, cognitive problems, and sensory abnormalities, which may be rooted in the disrupted development of the cerebral cortex, cerebellum, and the limbic system. Interestingly, abnormalities in olfaction have been reported in both ASD and schizophrenia, most often impairments in identification and discrimination of olfactory stimuli. Olfactory bulb is part of the limbic system and the first site of odor processing in the mammalian brain (Su et al., 2009). It relays olfactory information to other brain areas but also itself participates in odor recognition, discrimination, and odor-induced behavior (Su et al., 2009).

Finally, one more uniting feature of ASD and schizophrenia is the lack of effective treatments. At present, pharmacological interventions are inexistent in ASD and only partially effective in schizophrenia (Patel et al., 2014). For schizophrenia, a combination of psychotherapy and pharmacological therapy is often most effective (Patel et al., 2014). Pharmacological treatment is usually essential for the everyday functioning (Patel et al., 2014). Pharmacological options include several traditional and second-generation antipsychotics, however many patients suffering from schizophrenia do not respond to them (Patel et al., 2014). Clozapine is the most effective drug, but its significant disadvantage is the risk of developing agranulocytosis as well as electrolyte imbalances, both very dangerous side effects (Patel et al., 2014). In addition, there are unfortunately many patients who do not benefit from any medication (Patel et al., 2014). As for ASD, treatment is mainly limited to psychotherapy, although different medications have been tested and are used to alleviate specific symptoms and comorbidities accompanying the condition (DeFilippis and Wagner, 2016). Treatments of schizophrenia and especially those of ASD are currently only symptomatic, and

therapies that could cure these disorders do not exist. In the past decades, drug development in the field of mental disorder has generally appeared to be challenging to the pharmaceutical industry (Fibiger, 2012; Millan et al., 2016).

1.4 Research questions, hypotheses, and goals

The function of myosin XVI has begun to unravel, but many aspects of this myosin are still obscure. As described, several functions have been designated to it, but the publications are sparse and incoherent. This fact, together with the evidence that myosin XVI may play a role in ASD and schizophrenia, calls for elucidation of the very basic characteristics of myosin XVI to obtain a clearer picture of its function and biological relevance.

This Master's Thesis aimed to clarify the subcellular localization of myosin XVI. Where does myosin XVI localize in the cell? Does it co-localize with F-actin? These questions remain partly open in the current literature as the results from previous studies have been partly inconsistent. In order to elucidate this issue, human bone osteosarcoma epithelial (U2OS) cells endogenously expressing MYO16, and transfected U2OS cells overexpressing human MYO16B or rat Myo16b, were stained with different subcellular markers and imaged by epifluorescence microscopy. The hypothesis was that myosin XVI localizes in the cytoplasm and co-localizes with F-actin. These experiments sought to establish a better understanding of the localization of myosin XVI and to provide more insight into its function.

This thesis also aimed to clarify the developmental expression pattern of myosin XVI in the brain, concentrating on the olfactory bulb, hippocampus, cerebellum, and cerebral cortex. Is myosin XVI expressed in all these brain areas? Does the expression level differ between these brain regions and/or between developmental stages? According to the current literature, myosin XVI should be expressed in these regions, but description of the developmental expression pattern is missing, especially in the olfactory bulb. Previous studies suggest that myosin XVI expression and activity is highest in the perinatal days. In order to obtain insight into this issue, *Myo16*$^{+/+}$ (wild-type) and *Myo16*$^{-/-}$ (knock-out) mice of five different postnatal ages – postnatal day 1 (P1, newborn pup), P11 (infant pup), P28 (juvenile), P56 (young adult), and ~P250 (full-grown adult) – were utilized to perform western blotting. The hypothesis was that Myo16 is expressed in all these brain regions, and that the expression is higher early in the development. The ambition of these experiments was to determine the developmental trajectory of myosin XVI expression in the brain and whether and how myosin XVI is expressed in the developmental stages in which ASD and schizophrenia are manifested.

The ultimate goal of this Thesis was to enlighten the possible role of myosin XVI in the pathogeneses and symptoms of ASD and schizophrenia, with a particular interest in the olfactory bulb, a less studied brain structure in the context of neurodevelopmental disorders. Eventually, this research can open up new avenues for treatments, enabling development of more effective and targeted therapies for ASD and schizophrenia.

2 Results

2.1 Subcellular localization

2.1.1 Endogenous expression

To develop a better understanding of the function of myosin XVI, immunostaining and epifluorescence microscopy were employed in the examination of its subcellular localization. Endogenous expression of myosin XVI as well as overexpression of myosin XVIB in U2OS cells was verified by western blotting (see section 2.2.1 later in Results). First, endogenous expression of myosin XVI was studied by staining untransfected cells with four different anti-MYO16 antibodies, and the results varied depending on the antibody (**Figure 4**). Cells stained with MyBioSource anti-MYO16 displayed diffuse MYO16 localization mainly in the cytoplasm, especially in the perinuclear region. Proteintech anti-MYO16 showed MYO16 localization also mainly in the perinuclear region where the fluorescence was often enhanced in punctate structures, although not always. A less intense signal was also observed diffusely in the nucleus and cytoplasm. Biorbyt anti-MYO16 was found diffusely in the nuclei but also less intensely in the perinuclear region. Comparison with the secondary antibody control (Alexa Fluor 488 only) indicated that some signal observed with Proteintech and Biorbyt anti-MYO16 could be noise, because the secondary antibody showed minor diffuse labeling in the nuclei. Staining with Cameron et al.'s anti-MYO16 was very different from the three other antibodies, as it was typically restricted to the nuclei. None of the four studied anti-MYO16 antibodies suggested that endogenously expressed MYO16 clearly co-localizes with F-actin.

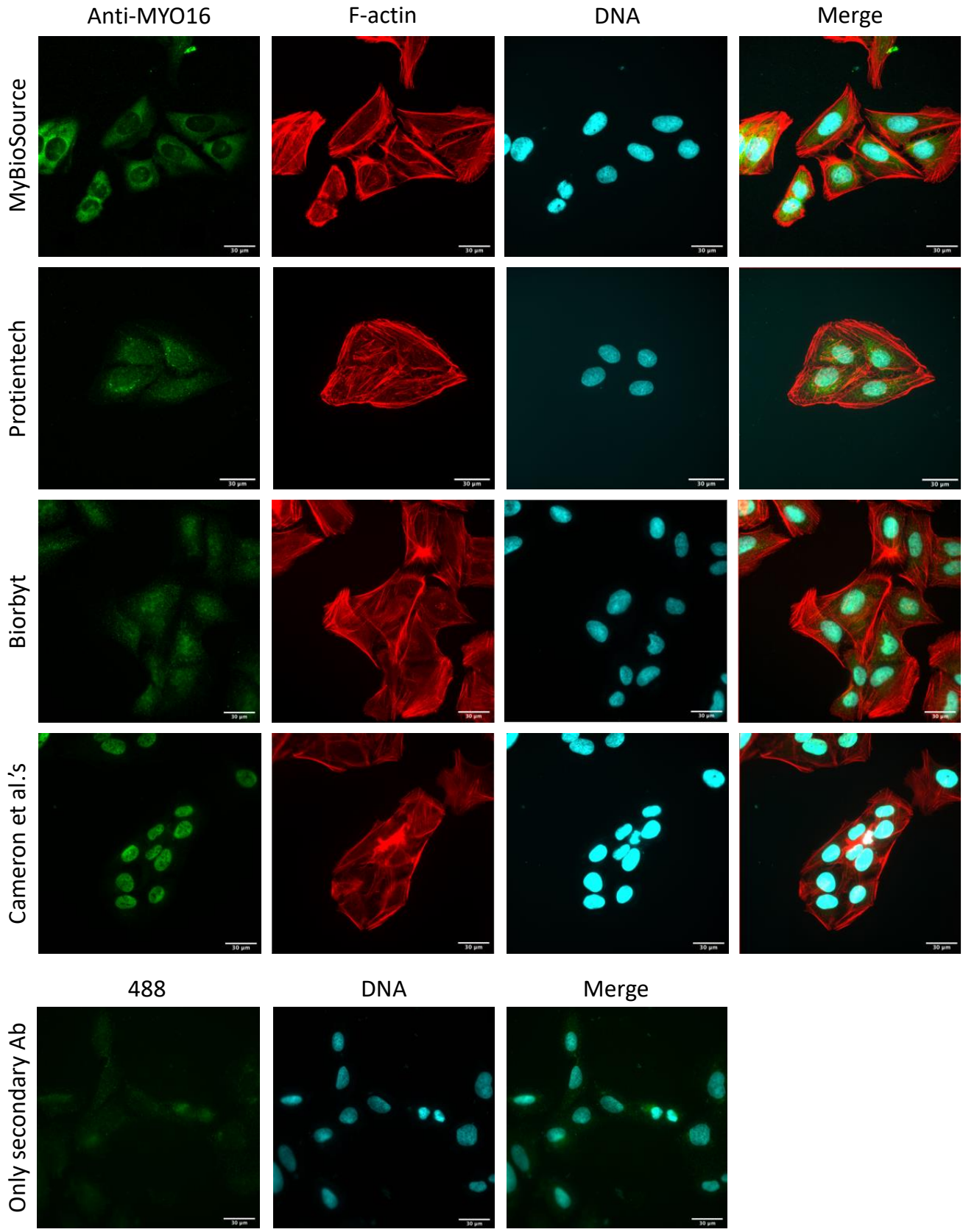

Figure 4. Untransfected U2OS cells stained with different anti-MYO16 antibodies (green), an F-actin marker (Alexa Fluor 594 phalloidin, red), and a DNA marker (DAPI, cyan), and untransfected U2OS cells stained with only secondary antibody (Alexa Fluor 488, green) and DAPI (cyan). Anti-MYO16 from antibodies top to bottom: MyBioSource anti-MYO16, Proteintech anti-MYO16, Biorbyt anti-MYO16, and Cameron et al.'s anti-MYO16. Scale bars: 30 μm. Objective: 63x.

A. MyBioSource anti-MYO16

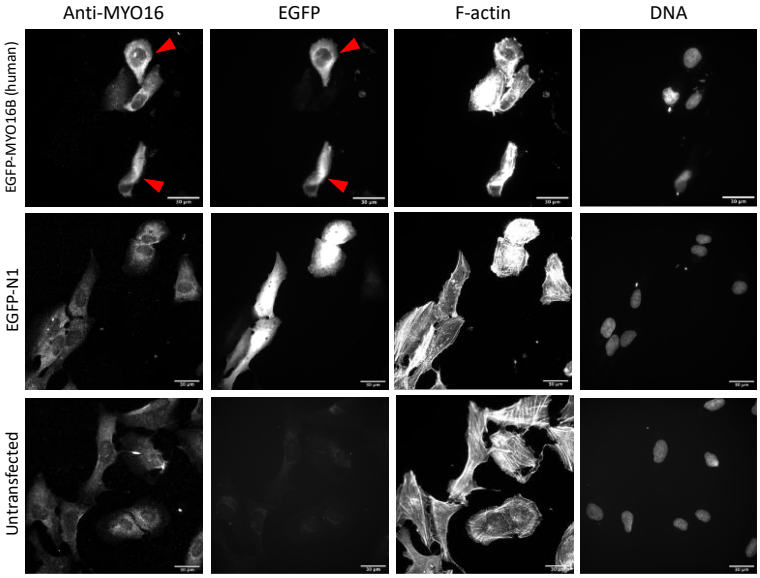

B. Proteintech anti-MYO16

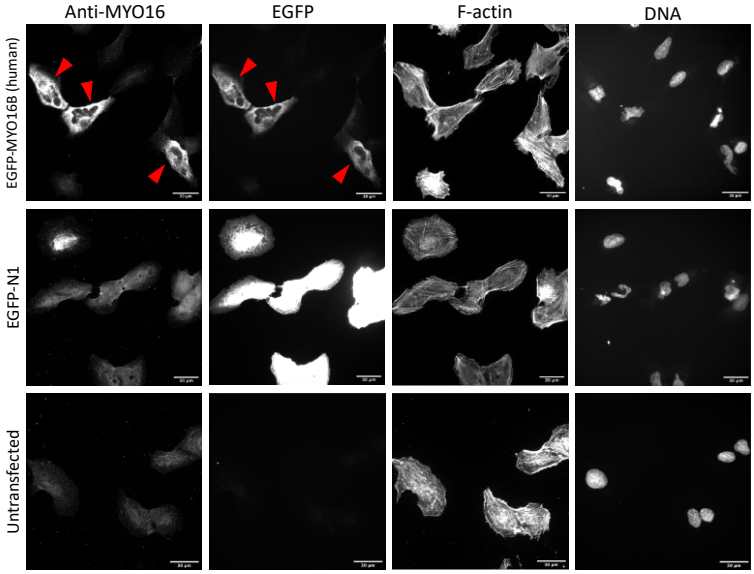

C. Cameron et al.'s anti-MYO16

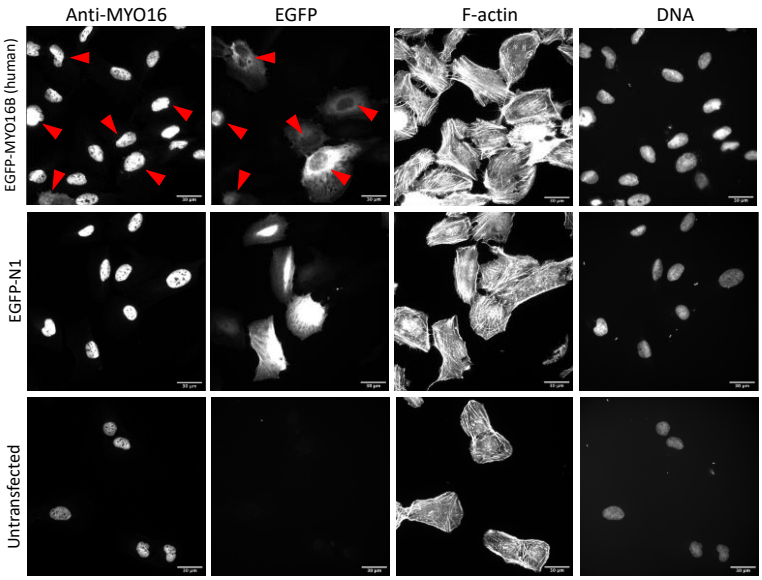

Figure 5. Human EGFP-MYO16B-overexpressing, EGFP-N1-overexpressing, and untransfected U2OS cells stained with different anti-MYO16 antibodies, an F-actin marker (Alexa Fluor 594 phalloidin) and a DNA marker (DAPI). **A**. MyBioSource anti-MYO16. **B.** Proteintech anti-MYO16. **C**. Cameron et al.'s anti-MYO16. EGFP-MYO16B-overexpressing cells are indicated with red arrowheads. Scale bars: 30 μm. Objective: 63x.

MyBioSource, Proteintech, and Cameron et al.'s anti-MYO16 were selected for further examination of the subcellular localization. To determine which of these antibodies, if any, was most reliably recognizing MYO16, transfected U2OS cells were stained with each antibody and co-localization of overexpressed MYO16 and anti-MYO16 staining was investigated (**Figure 5**). MyBioSource and Proteintech anti-MYO16 antibodies clearly recognized MYO16 overexpression, as the signal in human EGFP-MYO16B-overexpressing cells was similar to EGFP-MYO16B and also more intense than the signal in EGFP-N1-expressing and untransfected cells (Fig. 5A and B). MyBioSource anti-MYO16 stained EGFP-MYO16B-overexpressing cells similarly than EGFP-N1-expressing and untransfected cells, localizing to the cytoplasm (Fig. 5A). Proteintech anti-MYO16 stained EGFP-MYO16B-overexpressing cells slightly differently than EGFP-N1-expressing and untransfected cells, localizing to the cytoplasm or to the cytoplasm and nuclei, respectively (Fig. 5B). Cameron et al.'s anti-MYO16 did not recognize MYO16 overexpression as it localized to the nuclei, except for rare occasions when the antibody stained also the cytoplasm and co-localized with EGFP-MYO16B there (Fig. 5C). Despite these inconsistencies, all these three anti-MYO16 antibodies were chosen for closer investigation of the potential localization of MYO16, although the validity of Cameron et al.'s anti-MYO16 was questionable in the above experiment, at least in most cases.

When endogenous expression was examined using MyBioSource anti-MYO16, the anti-MYO16 displayed diffuse distribution in the cytoplasmic compartment where it was concentrated mainly to the perinuclear region (**Figure 6**). MyBioSource anti-MYO16 also frequently appeared in dots in the nucleus (Fig. 6; e.g., 6C). In addition, intense fluorescence signal was detected in the nuclei during cell division (Fig. 6E and F). As actin filaments were found principally in the cell periphery near the plasma membrane, the results indicated that endogenous MYO16 does not co-localize with F-actin (Fig. 6A, B, and D). However, co-localization might be possible during cell division when F-actin is also condensed in the nucleus, although this was difficult to confirm as the signals were too bright to distinguish the exact localizations.

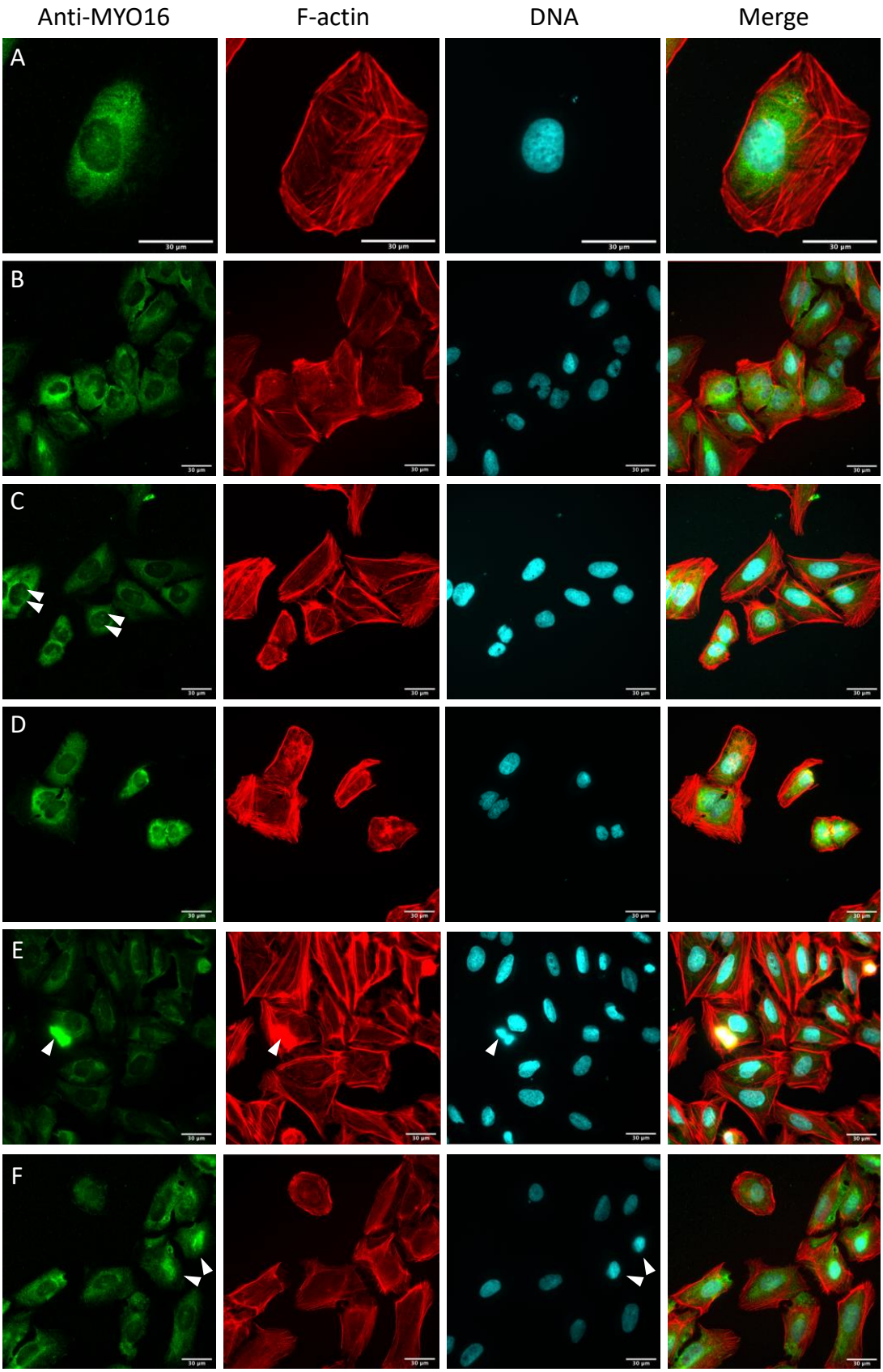

Figure 6. Untransfected U2OS cells stained with MyBioSource anti-MYO16 antibody (green), an F-actin marker (Alexa Fluor 594 phalloidin, red), and a DNA marker (DAPI, cyan). Scale bars: 30 μm. Objective: 63x. According to MyBioSource anti-MYO16, MYO16 is principally perinuclear (**A**–**F**). It sometimes appears in dots in the nuclei (**C**, white arrowheads), and might be also nuclear during cell division (**E** and **F**, dividing cells are denoted by white arrowheads), sometimes possibly co-localizing with F-actin there (**E,** white arrowheads).

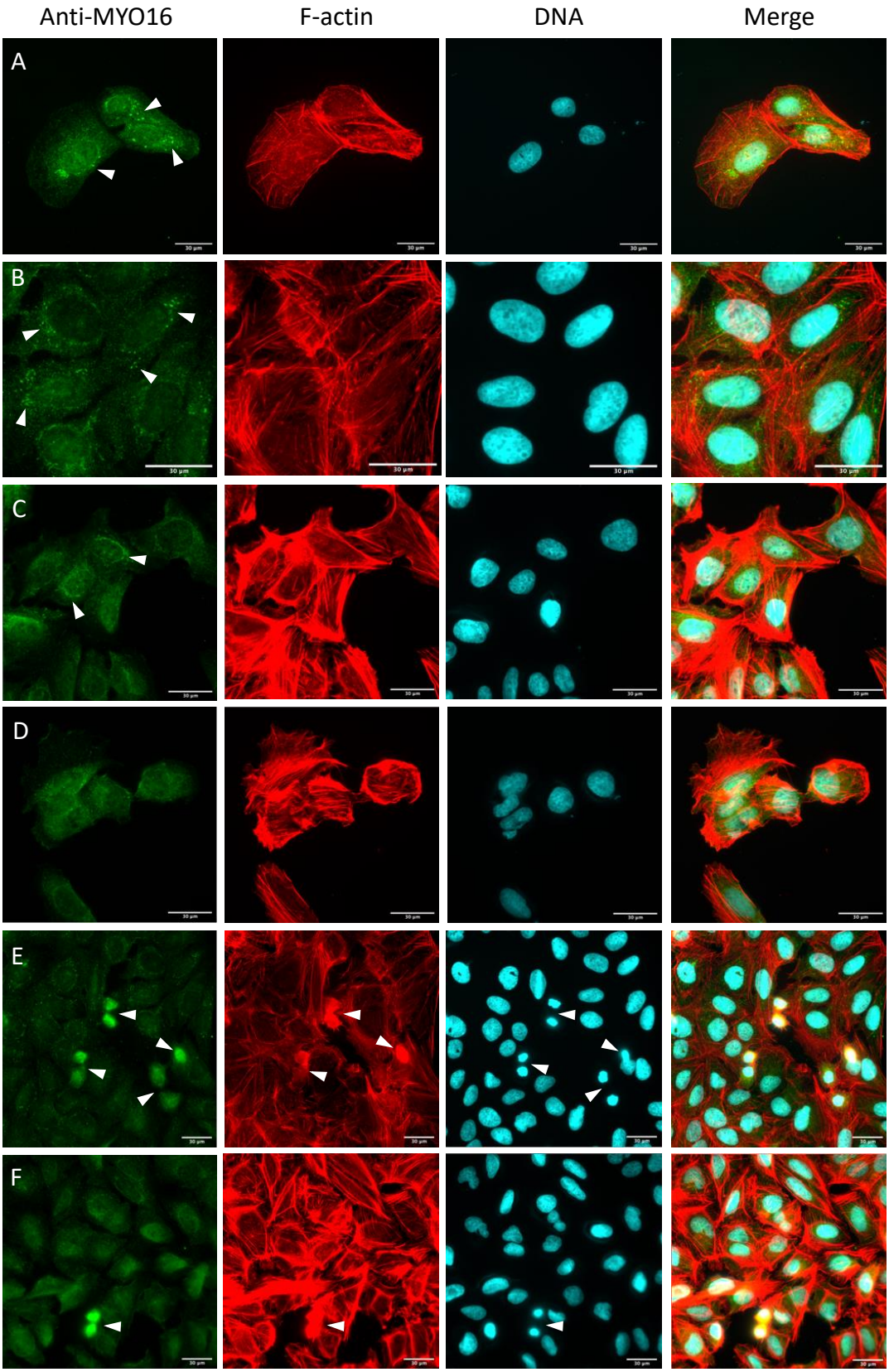

Figure 7. Untransfected U2OS cells stained with Proteintech anti-MYO16 antibody (green), an F-actin marker (Alexa Fluor 594 phalloidin, red), and a DNA marker (DAPI, cyan). Scale bars: 30 µm. Objective: 63x. According to Proteintech anti-MYO16, MYO16 is found quite diffusely in both the cytoplasm and in the nuclei (**A**–**F**). However, it is sometimes concentrated to the perinuclear region in a punctate manner (**A**–**C**, the puncta are denoted by white arrowheads). It may also appear in the nuclei during cell division and co-localize with F-actin there (**E** and **F**, dividing cells are denoted by white arrowheads).

Next, endogenous expression was examined using Proteintech anti-MYO16 (**Figure 7**). Proteintech anti-MYO16 displayed localization both in the cytoplasm and in the nucleus (Fig. 7; e.g., 7A). The fluorescence signal was typically most intense in the perinuclear region where it often appeared punctate (Fig. 7A–C). Sometimes the signal was however more diffuse and detected more widely in the cytoplasm (Fig. 7D). Different localization was again observed during cell division, when Proteintech anti-MYO16 was detected also in the nuclei (Fig. 7E and F). No apparent co-localization with F-actin was observed, but anti-MYO16 possibly co-localized with F-actin during cell division.

The third antibody, Cameron et al.'s anti-MYO16, revealed disctinctively different localization pattern than the two other anti-MYO16 antibodies (**Figure 8**). Cameron et al.'s anti-MYO16 was mostly restricted to the nucleus where the staining was diffuse and covered almost the whole nucleus, excluding some non-fluorescent spots that are likely the nucleoli (Fig. 8; e.g., 8A and B). Occasionally, Cameron et al.'s anti-MYO16 was detected in the cytoplasm as well (Fig. 8C and D). This seemed to occur during cell division (Fig. 7E). Cytoplasmic distribution was however not exclusive during cell division, as strong signal was also sometimes detected in the nuclei (Fig. 7F). Again, the anti-MYO16 only co-localized with F-actin potentially during cell division.

In summary, MyBioSource and Proteintech anti-MYO16 antibodies indicated that endogenous myosin XVI is generally cytoplasmic and usually enhanced in the perinuclear region, whereas Cameron et al.'s anti-MYO16 antibody suggested that myosin XVI is generally nuclear. However, all the antibodies implied that myosin XVI can be both cytoplasmic and nuclear during cell division.

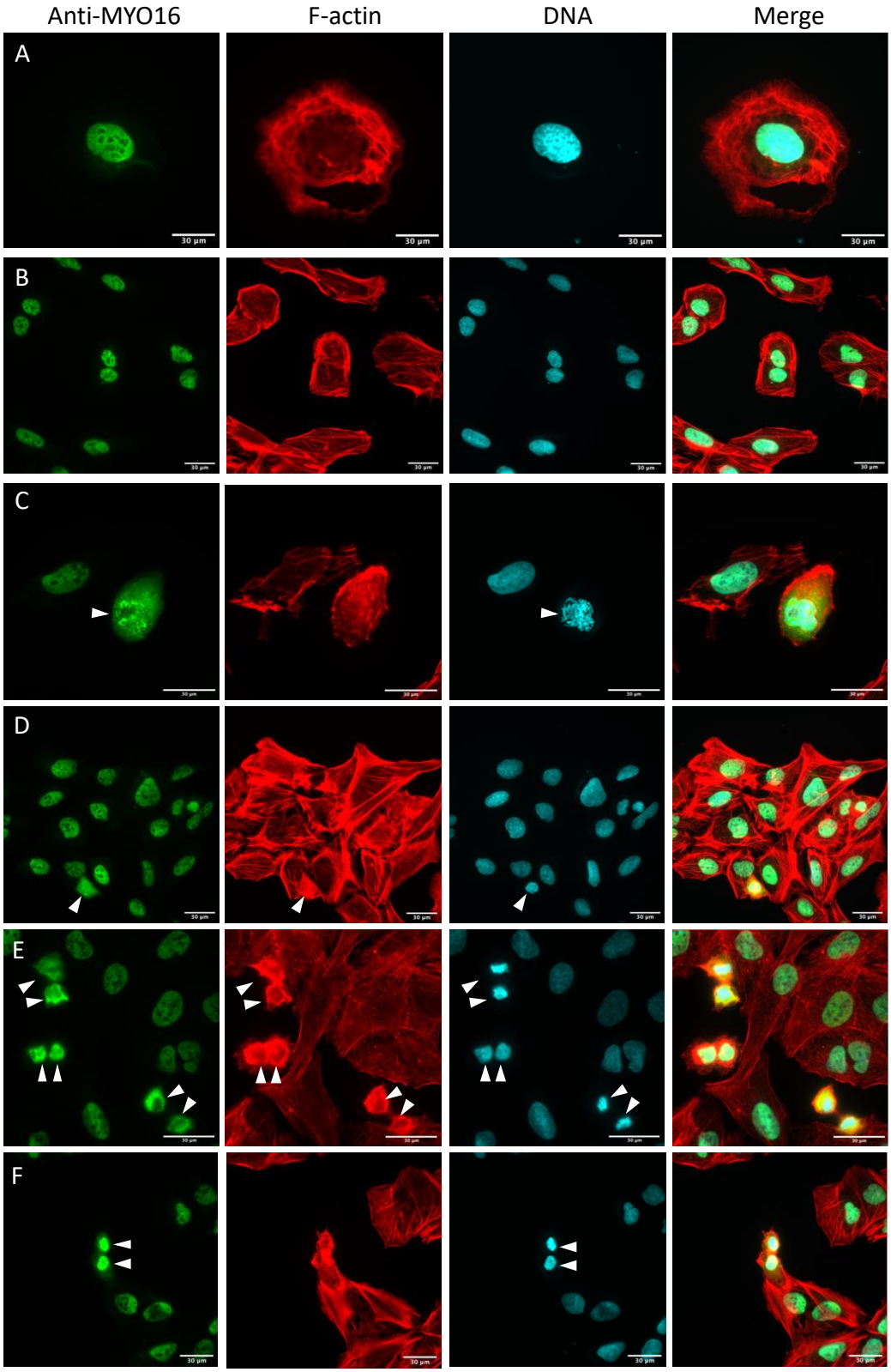

Figure 8. Untransfected U2OS cells stained with Cameron et al.'s anti-MYO16 antibody (green), an F-actin marker (Alexa Fluor 594 phalloidin, red), and a DNA marker (DAPI, cyan). Scale bars: 30 µm. Objective: 63x. According to Cameron et al.'s anti-MYO16, MYO16 is mainly nuclear and does not co-localize with F-actin (**A**–**F**). However, it sometimes appears in the cytoplasm well (**C** and **D**). During cell division, it may localize principally in the cytoplasm and co-localize with actin then (**E**, dividing cells are denoted by white arrowheads) or principally in the nuclei (**F**, white arroweheads).

2.1.2 Overexpression

Overexpression of myosin XVIB was studied using transfected U2OS cells stained with different subcellular markers. Transfection was successful, although transfection efficiency of human MYO16B-EGFP and rat Myo16b-EGFP was not as high as desired. This was likely due to the relatively large size of human pEGFP-*MYO16B* and rat pEGFP-*Myo16b* plasmids, both comprising around 240 kDa in protein size. Despite optimization of the Lipofectamine transfection protocol, many of the cells transfected with human MYO16B or rat Myo16b did not survive transfection. In addition to the transfection itself, this might indicate that overexpression of myosin XVIB is harmful to cells. Furthermore, dividing cells were less common among MYO16B/Myo16b-overexpressing cells than in untransfected cells, indicating that overexpression of myosin XVIB may cause problems in cell division.

Human EGFP-MYO16B and rat EGFP-Myo16b localized similarly in the U2OS cells; both distributed rather diffusely in the cytoplasm, concentrating most intensely in the perinuclear region and gradually decreasing in intensity towards the cell periphery (**Figure 9**). Cells expressing only EGFP-N1 displayed intense fluorescence throughout the entire cell.

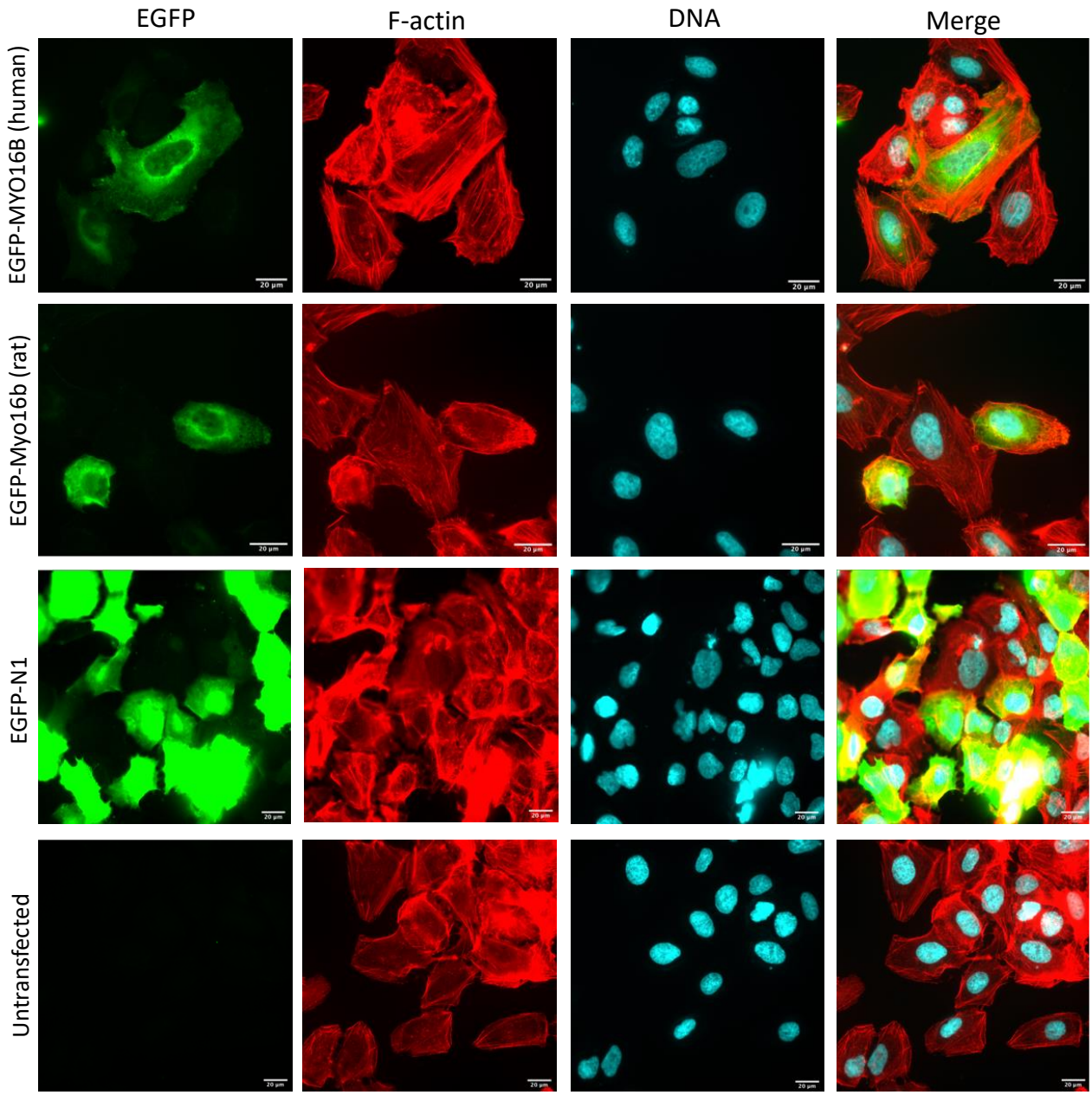

Figure 9. Overexpression of human EGFP-MYO16B, rat EGFP-Myo16b, and EGFP-N1 (positive transfection control) (green) in U2OS cells, and untransfected U2OS cells (non-treated control). The cells are stained with an F-actin marker (Alexa Fluor 594 phalloidin, red) and a DNA marker (DAPI, cyan) Scale bars: 20 µm. Objective: 63x.

A closer look at the subcellular localization of human EGFP-MYO16B, examined together with F-actin, revealed that EGFP-MYO16B localizes principally to the perinuclear region where F-actin is less abundant **(Figure 10**). Whereas actin filaments are most prevalent in the cell periphery where they are arranged vertically and horizontally in relation to the plasma membrane, EGFP-MYO16B was mostly detected perinuclearly (Fig. 10; e.g., 10F). In some occasions, however, EGFP-MYO16B was concentrated in some regions of the plasma membrane where it also appeared to co-localize with F-actin more clearly (Fig. 10A–C). These regions often resembled leading lamellipodia, but sometimes also retracting areas. Human MYO16-EGFP-overexpressing cells also seemed to be

especially motile, having large lamellipodia. EGFP-MYO16B generally displayed a fine punctate distribution pattern, but sometimes larger fluorescent aggregates that co-localized with F-actin were also seen (Fig. 10; e.g., 10E–G). These puncta could be vesicles or accumulated actin fibers, respectively. Moreover, EGFP-MYO16B was occasionally co-localized with F-actin in dots adjacent to or in the nucleus (Fig. 10D and H). These structures could be centrioles that are the main type of microtubule organizing centers (MTOCs) in cells. Additionally, increased fluorescence was sometimes observed between dividing cells, and it seemed that overexpression might disturb cytokinesis, perhaps by causing problems in squeezing the contractile ring between dividing cells (Fig. 10B).

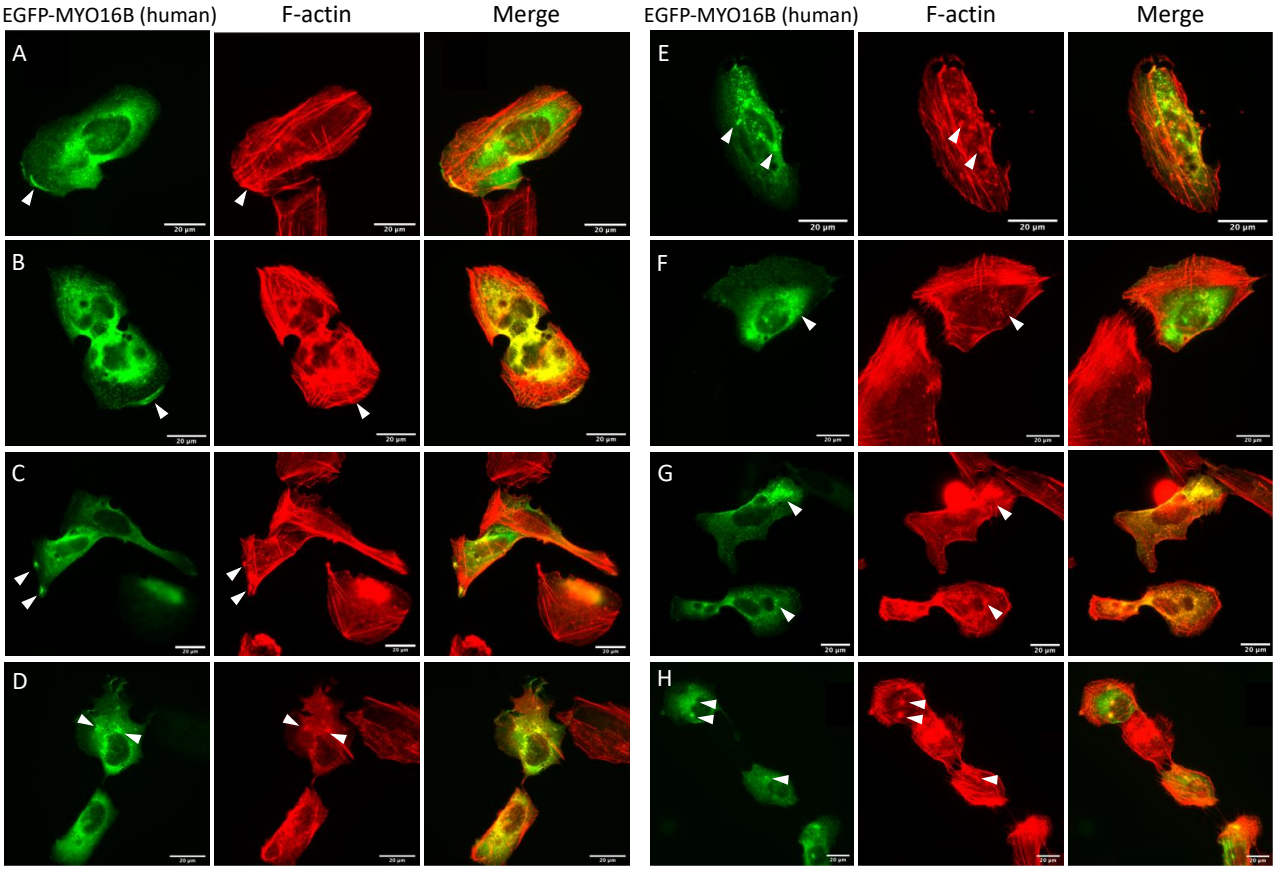

Figure 10. Human EGFP-MYO16B overexpression (green) in U2OS cells stained with an F-actin marker (Alexa Fluor 594 phalloidin, red). Scale bars: 20 µm. Objectives: 63x and 100x. EGFP-MYO16B appears to be distributed quite diffusely in small puncta in the cell (**A**–**H**). It is usually mostly concentrated to the perinuclear region where F-actin is less abundant (**A**, **B**, and **F**). It is sometimes found on the plasma membrane where clear co-localization with F-actin is observed (**A**–**C**, white arrowheads). Additionally, it may localize to larger or smaller cytoplasmic puncta that also co-localize with F-actin (**E** and **F**, white arrowheads), and is occasionally also found in dots adjacent to the nuclei (**D**, white arrowheads).

Similar to human EGFP-MYO16B-overexpressing cells, rat EGFP-Myo16b was also found principally in the regions where F-actin is less prevalent (**Figure 11**). Rat EGFP-Myo16b was most intense in the perinuclear region of the cytoplasm (Fig. 11A, E, and G). Similar to human EGFP-

MYO16B, rat EGFP-Myo16b was occasionally condensed in the plasma membrane on areas that were likely associated with membrane protrusion and migration, and there EGFP-Myo16b also overlapped with F-actin (Fig. 11A–D and H). The pattern of distribution was usually punctate, displaying fine-grained granules dispersed in the cytoplasm (Fig.11; e.g., 11G). As human EGFP-MYO16B, also rat EGFP-Myo16b was sometimes also observed in larger puncta, sometimes not overlapping with F-actin but sometimes co-localizing with it (Fig. 11E, F, and H).

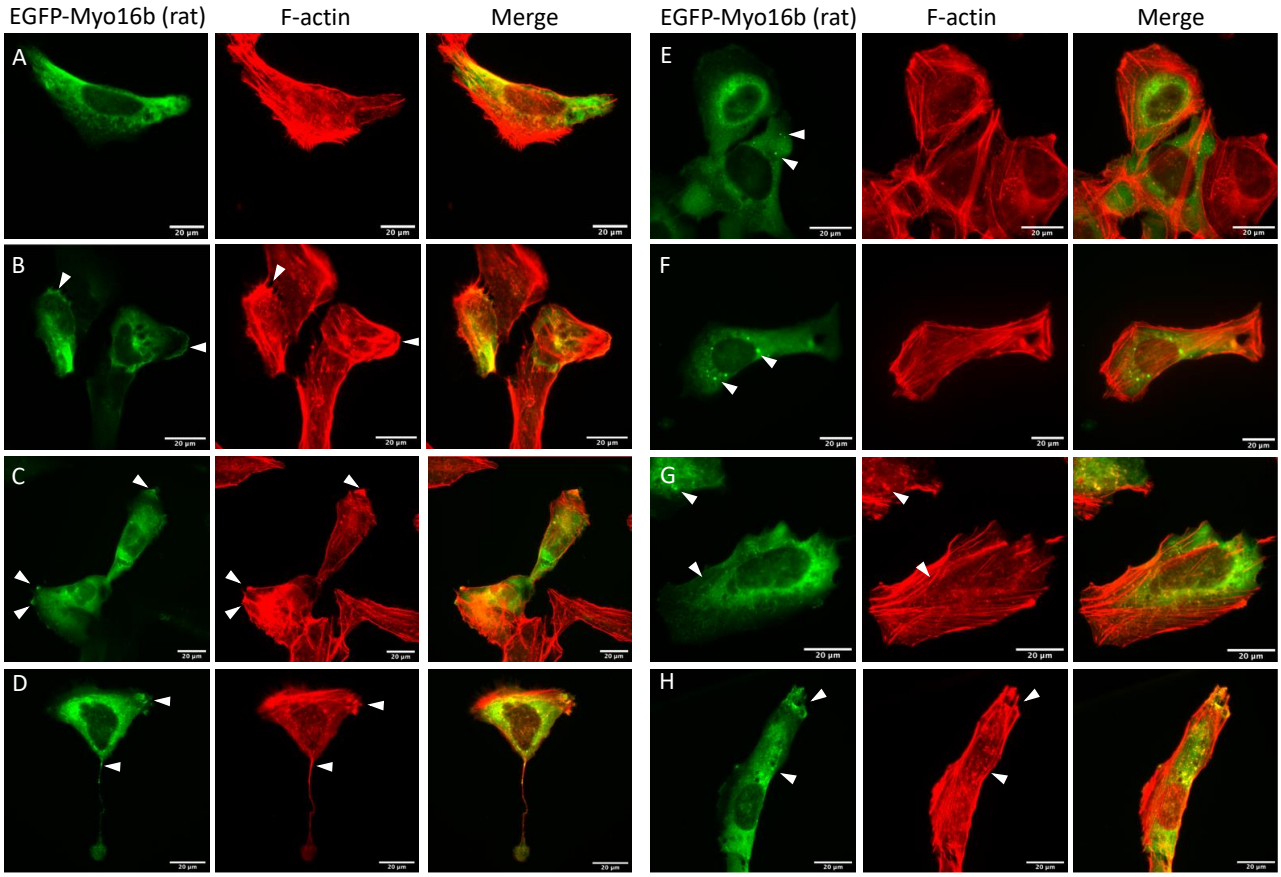

Figure 11. Rat EGFP-Myo16b overexpression (green) in U2OS cells stained with an F-actin marker (Alexa Fluor 594 phalloidin, red). Scale bars: 20 µm. Objectives: 63x and 100x. EGFP-Myo16b appears to be distributed rather diffusely in the cell (**A**–**H**). It often appears in the perinuclear region where F-actin is less abundant (**A**). It is sometimes found on the plasma membrane where it co-localizes with F-actin in membrane protrusions (**B**–**D**, white arrowheads). In addition, it localizes to larger cytoplasmic puncta that do not co-localize with F-actin (**E** and **F**, white arrowheads) or to smaller cytoplasmic puncta that co-localize with F-actin (**G** and **H**, white arrowheads).

To address whether the perinuclear distribution of myosin XVI overlaps with the endoplasmic reticulum (ER), transfected cells were stained with an ER marker, protein disulfide-isomerase (PDI) antibody (**Figure 12**). Both human EGFP-MYO16B and rat EGFP-Myo16b co-localized with some parts of the ER, and the EGFP signal was most intense in areas where the anti-PDI signal also appeared most intense (Fig. 12A–C).

To explore further the fluorescent dots observed adjacent to the nuclei of EGFP-MYO16B-overexpressing U2OS cells, the cells were stained with an MTOC marker; γ-tubulin antibody (**Figure 13**). This staining showed that EGFP-MYO16B may be localized to the centrosome, the major MTOC, in some occasions (Fig. 13A–C). However, this staining was not fully successful for the anti-γ-tubulin antibody, or then the antibody did not work ideally, based on the rather dim labeling of the centrioles and diffuse signal also elsewhere in the cell. This was likely not related to MYO16B/Myo16b overexpression either, as similar staining was observed in untransfected cells.

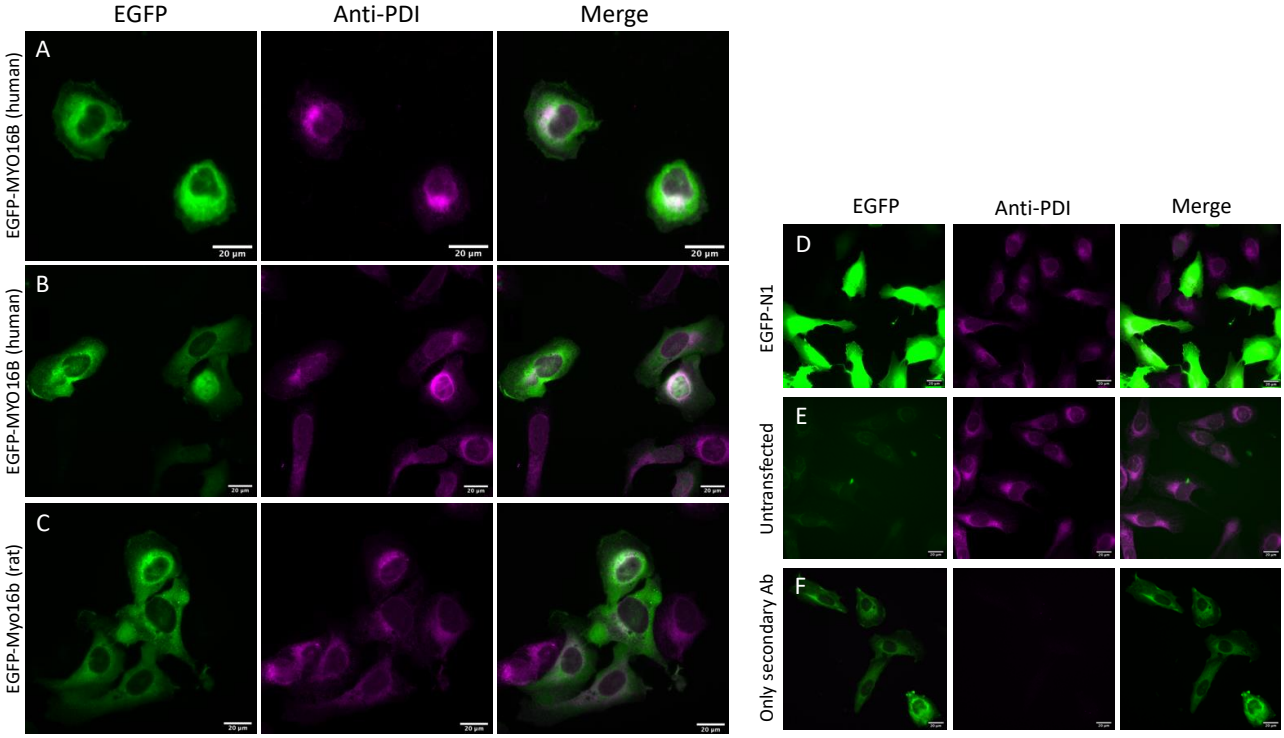

Figure 12. Co-localization of myosin XVIB and the endoplasmic reticulum (ER) in U2OS cells. **A** and **B**: Human EGFP-MYO16B overexpression (green) stained with an ER marker (anti-PDI, magenta). **C**: Rat EGFP-Myo16b overexpression stained with an anti-PDI. **D**: EGFP-N1 overexpression stained with an anti-PDI (positive transfection control). **E**: Untransfected cells stained with anti-PDI (non-treated control). **F**: Human EGFP-MYO16B overexpression stained with only secondary antibody (Alexa Fluor 647) (only secondary control). Scale bars: 20 µm. Objective: 63x.

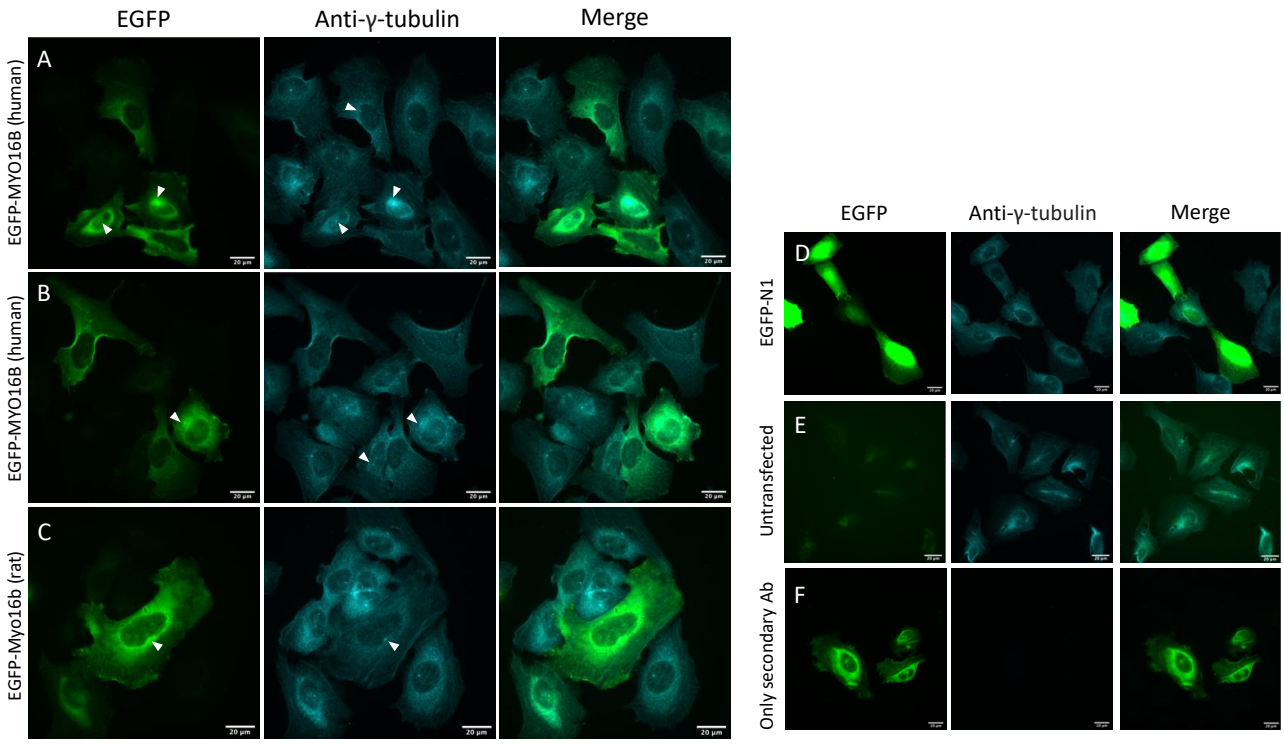

Figure 13. Co-localization of myosin XVI and microtubule organizing centers (MTOCs) in U2OS cells. **A**-**C**: Human EGFP-MYO16B overexpression (green) stained with an MTOC marker (anti-γ-tubulin, cyan). **D**: EGFP-N1 overexpression stained with an anti-γ-tubulin (positive transfection control). **E**: Untransfected cells stained with anti-γ-tubulin (non-treated control). **F**: Human EGFP-MYO16B overexpression stained with only secondary antibody (Alexa Fluor 647) (only secondary control). Scale bars: 20 µm. Objective: 63x.

In summary, overexpressed myosin XVIB localized mainly to the perinuclear region in U2OS cells. This distribution pattern and the localization of the endoplasmic reticulum were overlapping. The largely differential localization of F-actin implies that myosin XVIB does not widely interact with it, however occasional enhancement of myosin XVIB in the plasma membrane and the concurrent co-localization with F-actin suggest that myosin XVIB could interact with actin there, for example in lamellipodia. Moreover, myosin XVIB sometimes co-localized with F-actin in cytoplasmic puncta, possibly vesicles, indicating interaction there as well. Sometimes myosin XVIB appeared in dots adjacent to the nuclei, and these could be centrioles.

Localization pattern between overexpression and endogenous expression was partly consistent when comparing overexpression to endogenous expression studied with MyBioSource and Proteintech anti-MYO16 antibodies. In this case, both endogenous expression and overexpression were detected principally in the perinuclear region, although overexpression was also observed in other areas in the cell. However, if Cameron et al.'s anti-MYO16 is included in the comparison, the results from overexpression and endogenous expression become inconsistent as this anti-MYO16 was mainly concentrated in the nuclei.

2.2 Western blotting

2.2.1 Cell and mouse model validation and antibody selection

Western blotting was performed to confirm the expression of myosin XVI. First, expression of myosin XVI in U2OS cells and in Myo16 wild-type but not knock-out mice was verified. In addition, different anti-MYO16 antibodies were tested and the best one selected for subsequent western blotting experiments.

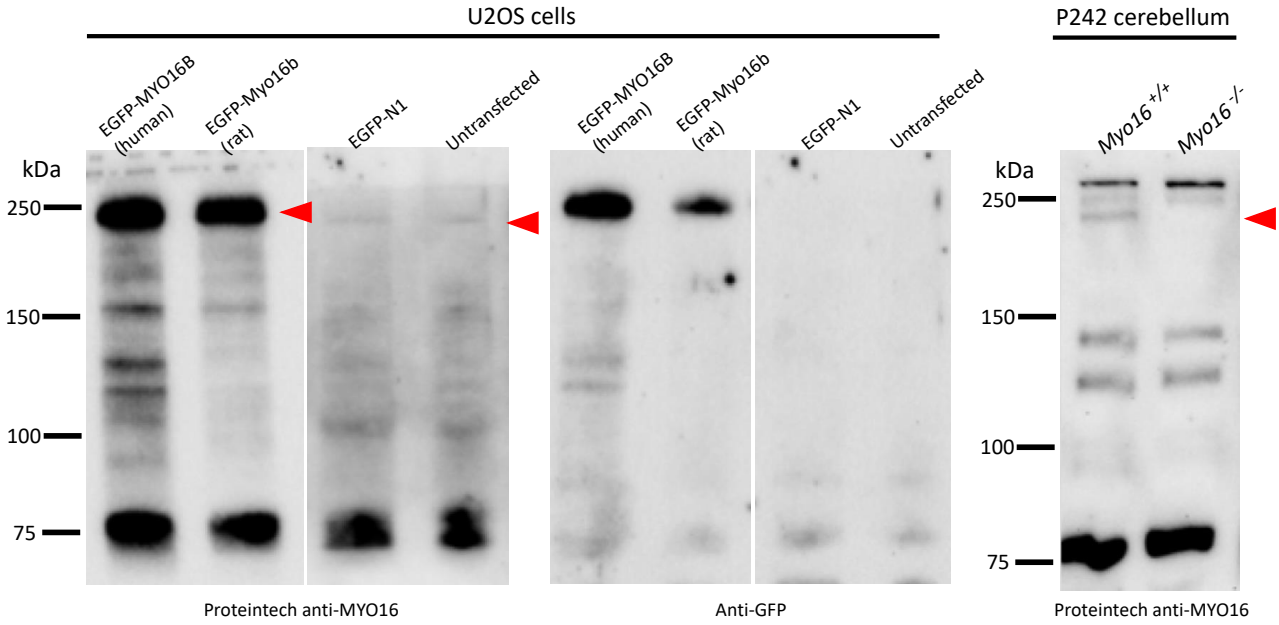

Figure 14. Confirming overexpression and endogenous expression of myosin XVI in U2OS cells and confirming Myo16 expression in P242 Myo16 wild-type (*Myo16*$^{+/+}$) and knock-out (*Myo16*$^{-/-}$) mouse cerebellum. P, postnatal day. Membranes with U2OS cell lysates were first incubated with Proteintech anti-MYO16, then stripped and incubated with anti-GFP (note: the size of EGFP-N1 is around 30 kDa and is not visible here). Membranes with mouse cerebellum homogenates were incubated with Proteintech anti-MYO16. U2OS cell lysates: 25 µg/well, mouse P242 cerebellum homogenates: 20 µg/well. Cell lysates were loaded in the same gel but presented here separately as the chemiluminescence detection time was different in Proteintech anti-MYO16 (the cells overexpressing myosin XVIB were overexposed quickly before the bands were visible in the cells endogenously expressing myosin XVI). Myosin XVIB bands are denoted by red arrowheads.

Western blotting for U2OS cell lysates and mouse brain homogenates firstly confirmed that Proteintech anti-MYO16 antibody recognizes myosin XVI, at least in this application (**Figure 14**). This experiment also confirmed that cells transfected with human pEGFP-*MYO16B* and rat pEGFP-*Myo16b* were overexpressing human EGFP-MYO16B and rat EGFP-Myo16b, respectively, as strong bands of around 250 kDa were detected in those lanes. In addition, the cells transfected with pEGFP-N1 and the untransfected cells were expressing MYO16B endogenously; bands of around 240 kDa were visible, though rather dim. Lastly, this experiment confirmed that Myo16b is expressed in Myo16 wild-type but not in Myo16 knock-out mice; bands of around 240 kDa were present in wild-

type mouse cerebellum but absent in knock-out cerebellum. These results verified that the U2OS cell line is suitable for studying endogenous as well as overexpression of myosin XVI, though the endogenous expression level may be quite low, and also confirmed the validity of the mouse model.

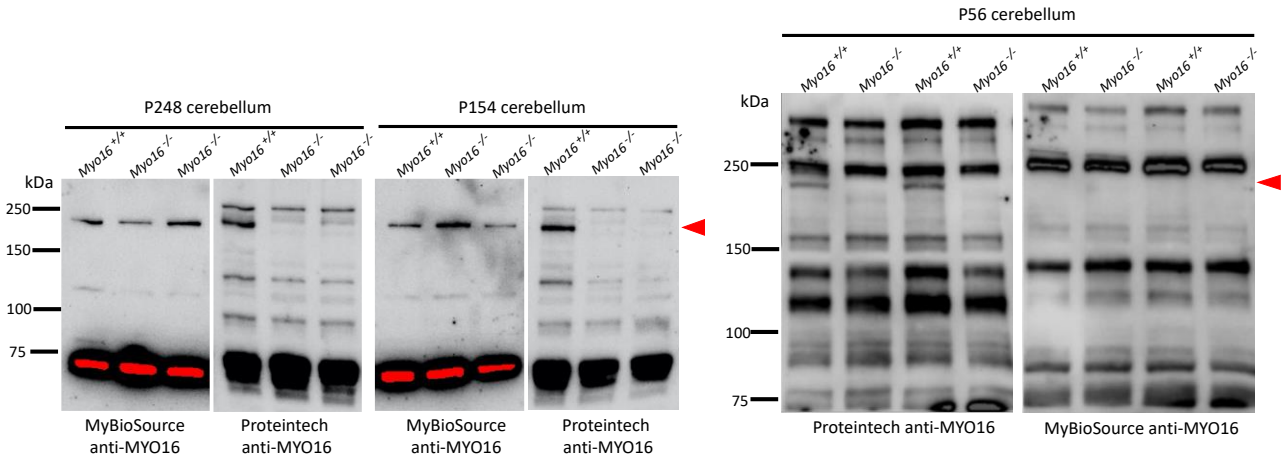

Figure 15. Comparison of Proteintech and MyBioSource anti-MYO16 antibodies in western blotting using P248, P154, and P56 Myo16 wild-type (*Myo16*$^{+/+}$) and knock-out (*Myo16*$^{-/-}$) mouse cerebellum samples. P, postnatal day. P248 and P154 cerebellum samples were first incubated with MyBioSource anti-MYO16 and then with Proteintech anti-MYO16, P56 cerebellum samples were first incubated with Proteintech anti-MYO16 and then with MyBioSource anti-MYO16. P248 and P154 cerebellum homogenates: 50 µg/well, P154 cerebellum homogenates: 20 µg/well. Myo16b bands are denoted by red arrowheads.

MyBioSource, Proteintech, and Cameron et al's anti-MYO16 antibodies were tested for western blotting. Cameron et al.'s anti-MYO16 was first excluded because we did not have much of it nor did it work as bands appeared also in knock-out mice. Results of MyBioSource and Proteintech anti-MYO16 showed that Proteintech anti-MYO16 was better applicable for western blotting; in the blots incubated with Proteintech anti-MYO16, bands were correctly visible in Myo16 wild-type but not in knock-out mice, whereas incubation with MyBioSource anti-MYO16 resulted in bands present in both wild-type and knock-out animals (**Figure 15**). Therefore, the Proteintech anti-MYO16 was selected for subsequent western blotting experiments. Unfortunately, Proteintech anti-MYO16 appeared to be quite unspecific especially in blots with samples from younger mice. The knock-out model proved to be a very important control to distinguish the protein band of interest. The additional bands were similarly present in wild-type and knock-out mice, indicating that they were not degradation products of Myo16b. According to the UniProtKB/Swiss-Prot database, mice may express another XVI isoform of around 200 kDa, however bands of this size were not observed in the blots. Non-specificity also led to another problem; gel electrophoresis needed to be run longer in order to separate Myo16 bands from unspecific bands of around the same molecular size, which resulted in proteins below 75 kDa to be moved out of the gel. As a consequence, common loading control proteins were not present in gels. Larger control proteins were not used because their

expression in the examined tissues was not clear, and gradient gels were also not readily available. This lack of loading control limited the quantifiability of myosin XVI expression. However, Myo16 band and total protein signals in each lane were measured and the Myo16–total protein ratio calculated in order to strengthen the reliability of results.

2.2.2 Myo16b expression in the olfactory bulb, hippocampus, cerebellum, and cerebral cortex

First, the expression of Myo16b in the mouse olfactory bulb, hippocampus, cerebellum, and the cerebral cortex was studied using wild-type (*Myo16*$^{+/+}$) and knock-out (*Myo16*$^{-/-}$) mice of five different ages: P1 (newborn pup), P11 (infant pup), P28 (juvenile), P56 (young adult), and P245 (full-grown adult) (**Figure 16**). The results confirmed that Myo16b is expressed in all these brain regions in all the studied ages. However, the expression was not uniform over the different regions. At P1, Myo16b appeared to be equally expressed in the olfactory bulb, hippocampus, and cerebellum. The expression in the cerebral cortex was lower compared to other regions. At P11, Myo16b seemed to be equally expressed in the olfactory bulb, cerebellum, and cerebral cortex, but was possibly less expressed in the hippocampus. Expression in the olfactory bulb may be slightly higher than expression in the cerebellum and cortex. At P28, Myo16b expression appeared to be highest in the olfactory bulb, second-highest in the cortex, and equally low in the hippocampus and cerebellum. At P56 and P245, Myo16b expression was highest in the olfactory bulb and clearly lower in the other regions. Lack of loading control limits the drawing of definitive conclusions, but the comparably high expression in the olfactory bulb in all ages was however repeatedly observed.

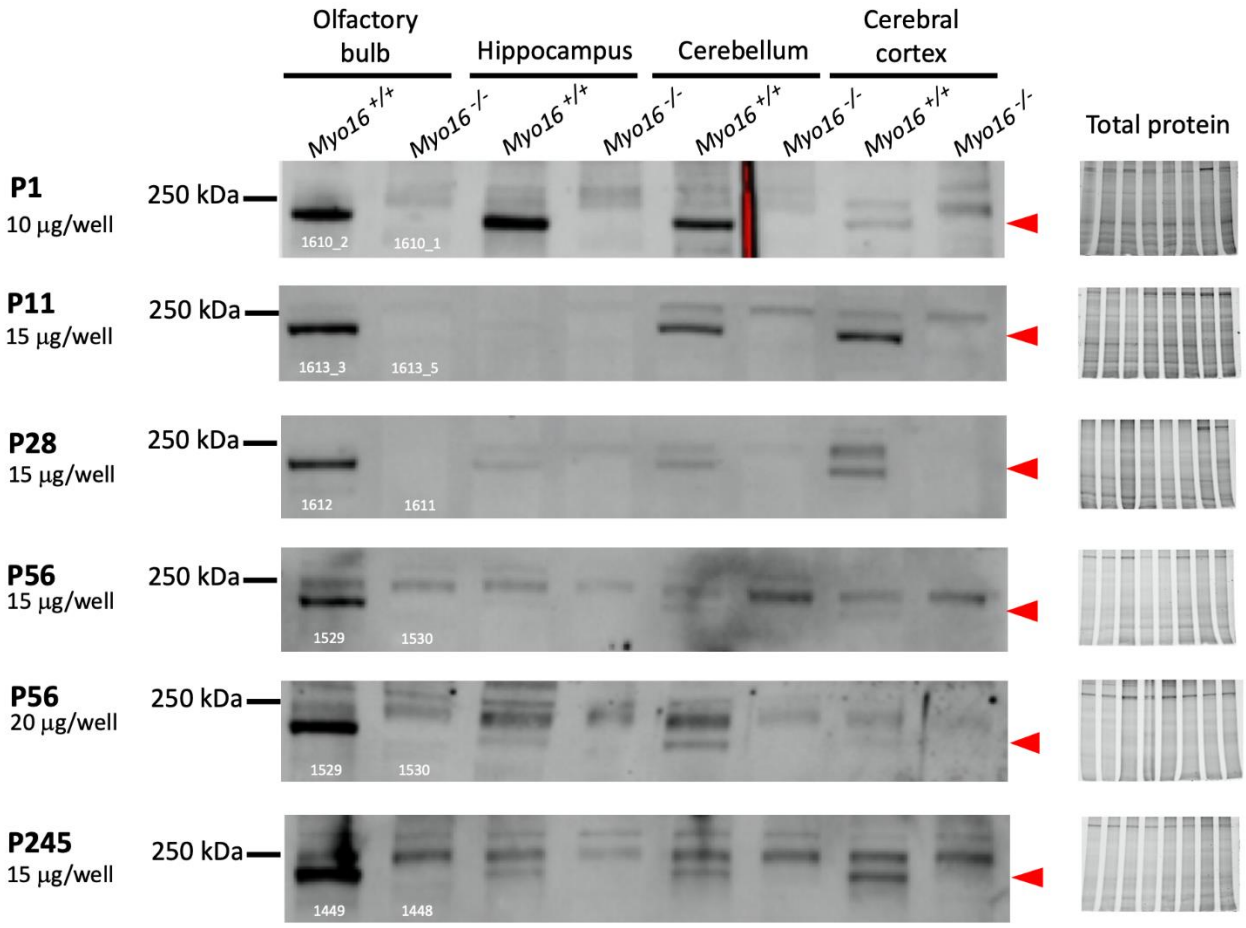

Figure 16. Myo16b expression in wild-type (*Myo16*$^{+/+}$) and knock-out (*Myo16*$^{-/-}$) mice in the olfactory bulb, hippocampus, cerebellum, and cerebral cortex at P1, P11, P28 (female), P56 (male), and P245 (female). P, postnatal day. P1: 10 µg/well. P11 and P28: 15 µg/well. P56 and P245: 15 µg/well. Samples from the same wild-type and knock-out mice were used for each brain region at each time point, and the wild-type and knock-out mice at each time point were from the same litter (identity numbers marked in white). Gels with total protein presented on the right. Myo16b bands are denoted by red arrowheads.

When Myo16b expression at P1 was compared between several wild-type animals, the expression seemed to vary between individuals in some regions (**Figure 17**). In the cerebral cortex, the expression was either considerably lower, little lower, or equal to the expression observed in the other regions (Fig. 17A). The expression was more equal in the olfactory bulb, hippocampus, and cerebellum (Fig. 17A), although some results also suggested that the expression in the olfactory bulb may also sometimes vary (Fig. 17B).

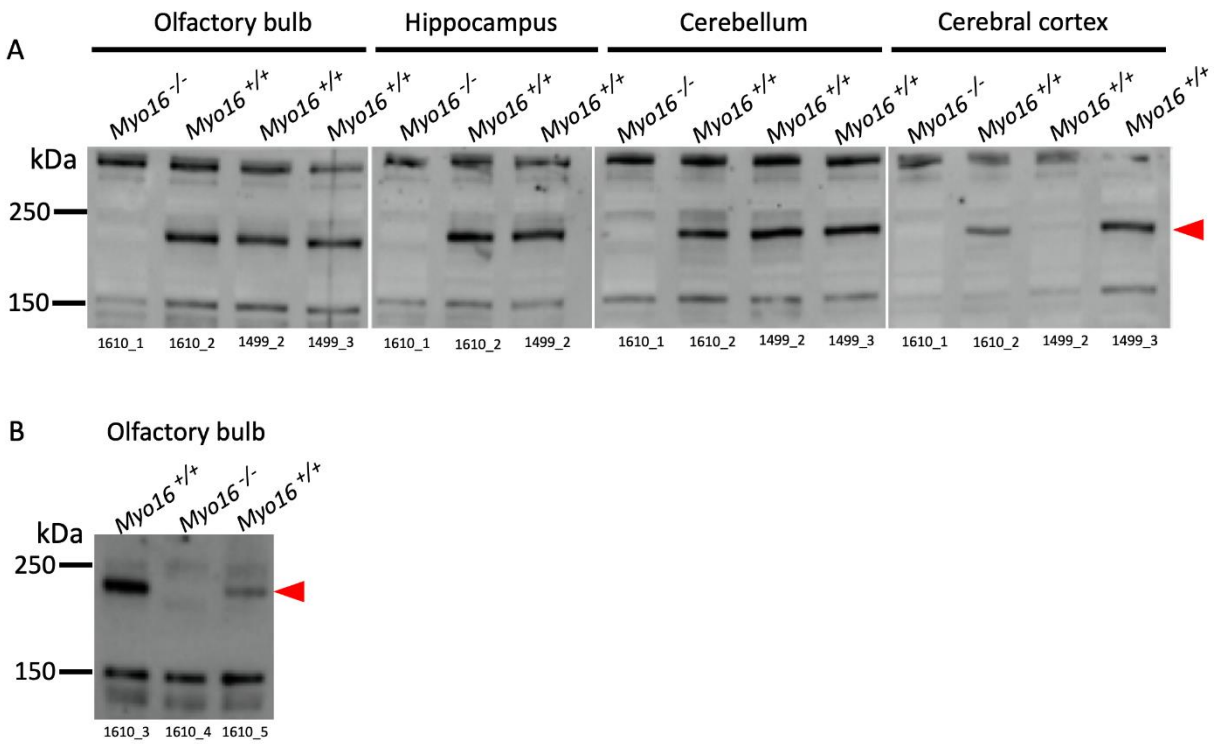

Figure 17. Myo16b expression at P1. **A**. Myo16 expression in the P1 olfactory bulb, hippocampus, cerebellum, and cerebral cortex. P, postnatal day. A knock-out (*Myo16*$^{-/-}$) mouse as a control and three wild-type (*Myo16*$^{+/+}$) mice expressing Myo16, 10 µg/well. Samples from the same wild-type and knock-out mice are used for each brain region in the same order (hippocampus from the last wild-type missing). **B.** Myo16 expression in the P1 olfactory bulb, 5 µg/well. Myo16b bands are denoted by red arrowheads. Identity numbers are marked below each lane.

To explore how the expression of myosin XVIB might change during the postnatal brain development, Myo16b expression in P1, P11, P28, and P56 wild-type mice was examined in the olfactory bulb, hippocampus, cerebellum, and cerebral cortex (**Figure 18**). Here, total protein and Myo16b band quantification were performed (Fig. 18B) in order to obtain more reliable results, and additionally the Myo16b–total protein ratio was calculated (Fig. 18C). This quantification appeared necessary, because the total protein was not always equal between the lanes. The results were largely consistent with those presented in Figures 16 and 17, indicating a more stable Myo16b expression in the olfactory bulb compared to the other regions (Fig. 18A and C). There might, however, be a temporary decline in Myo16b expression at P28, and the expression may even be higher in adult than in infant mice (Fig. 18C). In the hippocampus, Myo16b expression at P1 and P11 was variable, being high in some P1 and P11 mice but lower in others, however low expression at P28 and P56 was a consistent finding (Fig. 18A and C). Overall, it seems that the expression tends to be higher in infant mice than in juvenile and adult mice (Fig. 18C). In the cerebellum and cortex, Myo16b expression was higher at P1 and P11 compared to P28 and P56, indicating a higher expression early in development and a subsequent decline (Fig. 18A and C). This difference was however smaller in the cerebellum than in the cortex where the difference was clearer (Fig. 18C).

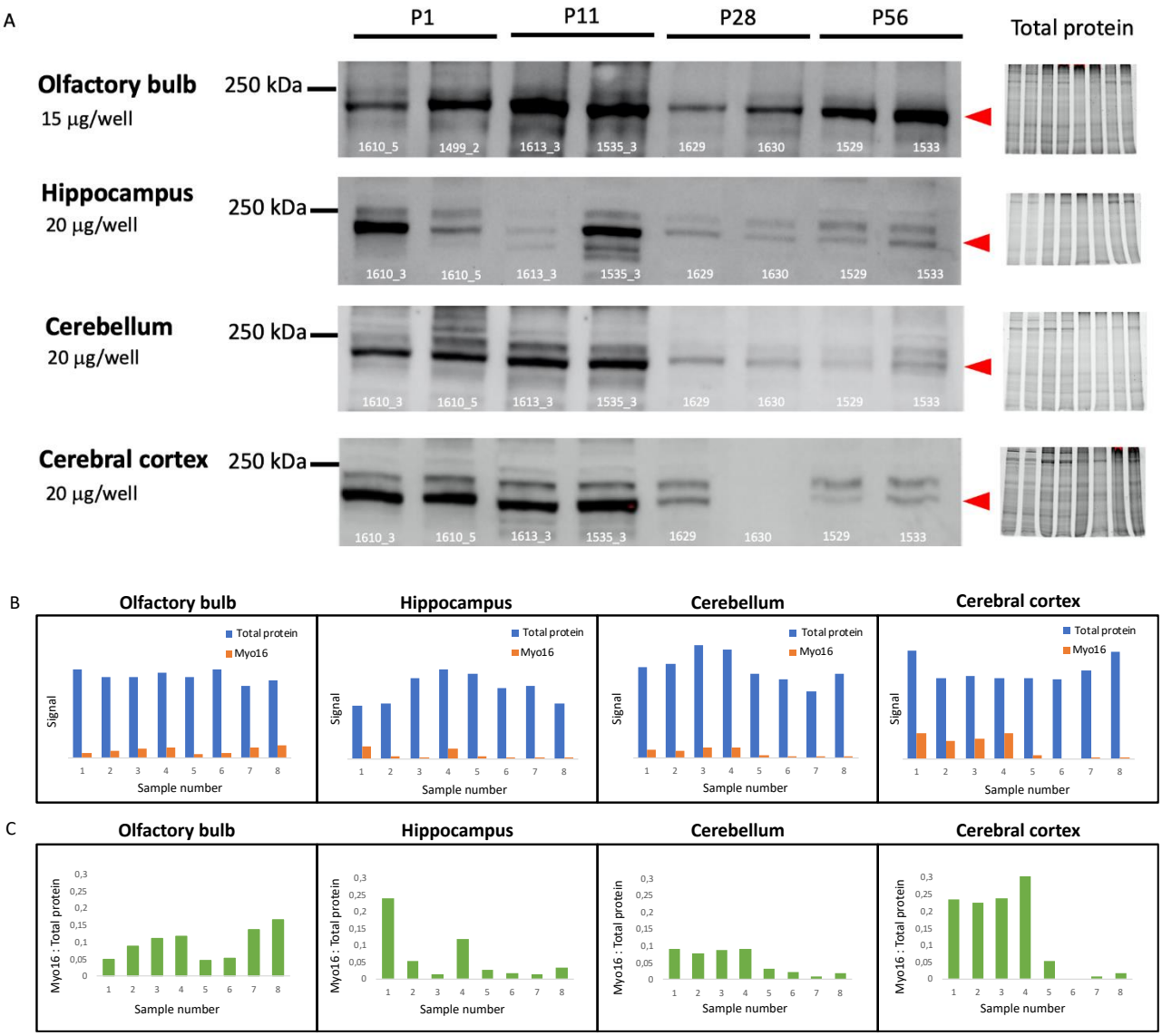

Figure 18. Developmental expression pattern of Myo16b in mouse olfactory bulb, hippocampus, cerebellum, and cerebral cortex. **A**. Expression of Myo16b in wild-type (*Myo16*$^{+/+}$) olfactory bulb, hippocampus, cerebellum, and the cerebral cortex at P1, P11, P28 (male), and P56 (male). P, postnatal day. Olfactory bulb: 15 µg/well. Hippocampus, cerebellum, and cerebral cortex: 20 µg/well. Gels with total protein presented on the right. Except for P1 olfactory bulb, samples from the same wild-type pairs are used for each developmental time point in each brain region (identity numbers marked in white). Myo16b bands are denoted by red arrowheads. **B**. Comparison of total protein (blue) and Myo16b (orange) signals in each sample (the samples are numbered from 1–8 but are in the same order as in A). **C**. Myo16b–total protein ratio in each sample (the samples are numbered from 1–8 but are in the same order as in A).

Some results not presented here indicated that there might be differences in Myo16b expression between male and female mice. The sex of pups (P1 and P11 animals) was not determined due to methodological issues, but the sex of the older animals (P28, P56, and ~P250) was known. It is worth noticing that the differing results observed between P1 and P11 animals could be due to sex differences although this was not possible to be examined here.

3 Discussion

3.1 Subcellular localization of myosin XVI

The first aim of this Master's Thesis project was to elucidate the subcellular localization of myosin XVI. Co-localization with F-actin was of particular interest. To illuminate this, both endogenous expression and overexpression of myosin XVI were explored in U2OS cells. The hypothesis was that myosin XVI localizes in the cytoplasm and co-localizes with F-actin.

With respect to endogenous expression, MyBioSource and Proteintech anti-MYO16 antibodies displayed MYO16 localization mainly in the cytoplasm and often concentrated to the perinuclear region. Human EGFP-MYO16B and rat EGFP-Myo16b overexpression also distributed in the cytoplasm and concentrated principally to the perinuclear region where overexpression partly overlapped with the ER. Enhanced fluorescence was also detected in small cytoplasmic puncta, where it often overlapped F-actin. In addition, Proteintech anti-MYO16 was frequently accumulated in a punctate manner to the perinuclear region. In line with these results, previous studies have observed myosin XVI in the neuronal cytoplasm in a punctate manner (Patel et al., 2001), and human and rat myosin XVIB overexpression in the cytoplasm distributing either diffusely throughout it or to the perinuclear region in a punctate fashion (Cameron et al., 2007). Although the perinuclear region is not the primary site of F-actin, it is present there (Svitkina, 2018). The perinuclear region is one site of the endomembrane system, a dynamic set of interconnected cytoplasmic membranes that together function as an intracellular transportation machinery between the nucleus and the plasma membrane (Dacks et al., 2009). In eukaryotes, the main components of the endomembrane system are the nuclear membrane, rough and smooth ER, Golgi apparatus, lysosomes, endosomes, vesicles, and the plasma membrane (Dacks et al., 2009). The Arp2/3 complex is known to be localize to the endomembrane system as well (Goley and Welch, 2006). Therefore, it is not too far-fetched to hypothesize that also myosin XVI, a regulator of the Arp2/3 complex, may operate in the endomembrane system and contribute to vesicle traffic, for instance. Supporting this idea, myosin XVI has been described to localize in vesicles in SH-SY5Y cells (The Human Protein Atlas), and one study has found that myosin XVI is important for the number of synaptic vesicles in neurons (Roesler et al., 2019). Several other myosins are also known to localize in different parts of the endomembrane system and interact with actin there (Hartman and Spudich, 2012). For example, myosin VA appears to be important for recycling of endosomes in neurons, and VB transports the ER to dendritic spines in cerebellar Purkinje cells (Wagner et al., 2011; Wang et al., 2008).

Moreover, large and intensely fluorescent cytoplasmic aggregates were observed in the cell overexpressing myosin XVIB. A previous study has indicated that overexpression of myosin XVI in HeLa cells may result in collapsed actin filaments and cause their accumulation in the cytoplasm (Yokoyama et al., 2011). The observed aggregates might be these, indicating that overexpression of myosin XVI can lead to disturbances in the organization of cytoplasmic actin filaments.

In the current study, overexpression of myosin XVIB was also observed in some regions of the plasma membrane where it often co-localized with F-actin. These regions often resembled lamellipodia but also retracting areas. Myosin XVIB has been detected in the underlying surface of the plasma membrane also in neurons (Patel et al., 2001) and the myosin XVIB tail domain has also been detected in lamellipodia and filopodia in COS-7 cells (Cameron et al., 2007). The Arp2/3 complex is also present there, regulating the reorganization of lamellipodia, for example (Goley and Welch, 2006). This indicates that myosin XVIB has an associated role there as well. Formation of membrane protrusions is crucial for cell migration, morphogenesis, and neurite outgrowth, as well as for the formation of synapses and dendritic spines (Flynn, 2013). Previously, myosin XVI has been implicated in all of these functions (Patel et al., 2001; Roesler et al., 2019; Yokoyama et al., 2011).

Intense fluorescence was also sometimes detected in puncta adjacent to, or inside, the nuclei when myosin XVIB was overexpressed. Interestingly, the results also indicated that myosin XVIB overexpression may disturb cell division. MyBioSource anti-MYO16 also occasionally appeared in nuclear dots. The observed dots could be centrioles, based on the staining with anti-γ-tubulin. Centrioles form the centrosome, an organelle found close to the nucleus (Sanchez and Feldman, 2017). The centrosome is essential for the alignment of chromosomes during cell division, for example, and for progression of the cell cycle (Sanchez and Feldman, 2017). Although the main component of the centrosome is tubulin, also actin is associated with it (Rosenblatt et al., 2004). Interestingly, also the Arp2/3 complex possibly transiently localizes to the centrosome during the interphase (Hubert et al., 2011). It is therefore possible that myosin XVI regulates centrosomal function. Myosins II and V are also known to associate with the centrosome (Espreafico et al., 1998; Rosenblatt et al., 2004).

There is also evidence that myosin XVI plays a role in cell cycle progression inside the nucleus. Earlier studies suggest that is required for completion of the interphase before the cell can continue to cell division (Cameron et al., 2007; Cameron et al., 2013). This is supported by the findings that 1) Myo16 is nuclear during interphase but both nuclear and cytoplasmic during cell division, 2) the expression level of Myo16 is higher during interphase and reduced during cell division, 3) Myo16-

deficient cells exhibit abnormal morphology as well as features characteristic to apoptosis, and 4) overexpression of Myo16b suppresses cell proliferation (Cameron et al., 2007; Cameron et al., 2013). Not surprisingly, Cameron et al.'s anti-MYO16 – the same one used to arrive at the above-listed conclusions – suggested a major localization to the nucleus and partial spreading to the cytoplasm during cell division in the present study. MyBioSource and Proteintech anti-MYO16 antibodies also seemed to localize to the nucleus during cell division despite their principal localization to the cytoplasm. Previously, in addition to their cytoplasmic locations, human and rat myosin XVIB overexpression have been observed also in the nucleoplasm – distributing either uniformly or in puncta (Cameron et al., 2007) – a finding not replicated in in this study. The precise molecular mechanisms behind the alternating locations of myosin XVI are currently unclear, however. The C-terminal tail domain of myosin XVIB contains an NLS sequence and is considered to mediate localization to the nucleus, whereas the N-terminal pre-motor domain contains an NES sequence and could therefore mediate localization to the cytoplasm (Cameron et al., 2007). Although F-actin is principally found in the cytoplasm, it is also present in the nucleus, at least transiently during cell division, indicating that myosins may interact with F-actin there as well (Baarlink, 2017).

The localization of myosin XVI is likely dependent on the phase of the cell cycle, but the observed locations of endogenous expression may also be influenced by other factors. First, post-translational modifications could affect antibody binding. For example, Cameron et al.'s anti-MYO16 could recognize MYO16 when it is modified to a form present in the nucleus. Second**,** non-specificity of the antibodies is always a concern. Unfortunately, the anti-MYO16 antibodies used in the current study were not completely specific to myosin XVI in western blotting, which indicates the same in staining. Finally, although myosin XVIA isoform should be expressed less than the XVIB isoform in the body, it is also likely present in smaller quantities, and the antibodies possibly tagged it as well. All the anti-MYO16 antibodies used in this study bound N-terminal sequences not specific to myosin XVIB; MyBioSource and Cameron et al.'s anti-MYO16 tagged sequences from the motor domain and Proteintech anti-MYO16 a sequence from the pre-motor domain. However, myosin XVIA has been reported to localize to the cytoplasm only and concentrate to the perinuclear region similarly to myosin XVIB there (Cameron et al., 2007). Expressing N- and C-termini of myosin XVI separately might however help to elucidate the differing locations.

The present results of subcellular localization of myosin XVI are summarized in **Figure 19**. Whether the observed locations are reproducible in other cell types, such as in neurons, remains a question that future studies need to answer. Obtaining a consistent understanding of the subcellular localization of

myosin XVI – whether nuclear, cytoplasmic, or both, and whether dependent on the cell type – will further clarify its function and biological significance. The possible role of myosin XVI in cell division and cell migration could be studied using live cell imaging. Exploring co-localization with the PI3K, WRC complex, and Arp2/3 complex, for example, would possibly enable more solid conclusions of the cellular mechanisms and function of myosin XVIB.

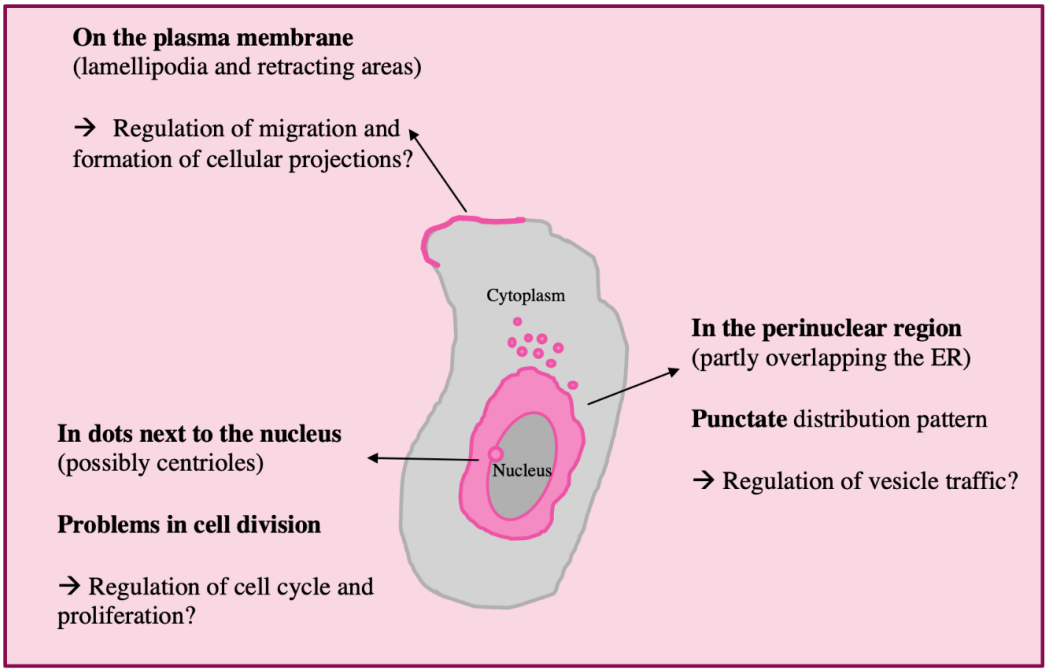

Figure 19. Graphical summary of subcellular localization results and proposed functions for myosin XVI.

3.2 Myo16b expression in the brain

The second aim of this Master's Thesis was to study Myo16 expression in different regions of the mouse brain, and to elucidate the expression trajectory of myosin XVI during postnatal brain development. The hypothesis was that Myo16b is expressed in all the studied regions, but we expected that the expression is highest at P1 and gradually decreased in later stages.

Western blotting confirmed that Myo16b is expressed in the olfactory bulb, hippocampus, cerebellum, and cerebral cortex from newborn to full-grown adult mice. This finding was aligned with earlier reports that have confirmed the presence of Myo16 mRNA and protein in these areas in young rodents (Patel et al., 2001; Yokoyama et al., 2011). This study confirmed that Myo16b is expressed also in older adult mice.

With respect to the hippocampus, cerebellum, and cortex the present results also indicated a higher Myo16b expression in P1 and P11 pups compared to juveniles (P28) and young adults (P56). The

developmental expression pattern in the olfactory bulb was an exception, showing more stable Myo16b expression also after the early postnatal days. Myosin XVI expression is reportedly highest during the early postnatal days (Patel et al., 2001; Yokoyama et al., 2011). For example, the level of Myo16 mRNA expression in rat cerebellum and cortex peaks during the first and second postnatal weeks (Patel et al., 2001). Interestingly, phosphorylation of the tyrosine residues of mouse Myo16b begins in the embryonic period, peaks during the perinatal days, then gradually decreases, and is significantly lower in adult animals (Yokoyama et al., 2011). This suggests that myosin XVIB is most active during this period, at least in respect to activation of the PI3K–WRC–Arp2/3 pathway and consequent branched actin formation that are assumedly triggered by phosphorylation of myosin XVIB (Yokoyama et al., 2011). Next, it would be interesting to determine the phosphorylation state of Myo16b from the blots of this study as phosphatase inhibitors were used in all samples.

The specific functions of myosin XVI in the developing brain remain elusive. Yokoyama et al. (2011) found that mouse Myo16 localizes to developing cortical neurons during the embryonic period. In P10 rat brain, Myo16b localizes to migrating cerebellar granule neurons (Patel et a., 2001). A recent study found that Myo16 localizes to the dendritic spines in the mouse cerebellum (Roesler et al., 2019). These findings, also supported by the results indicating localization to the plasma membrane and vesicles, provide evidence that myosin XVI regulates cell migration and synaptic function. Also consistent with these hypotheses, actin cytoskeleton reorganization is crucial for many neurodevelopmental processes, such as migration, neurite outgrowth, and formation of synapses and dendritic spines (Andersen, 2003; Yokoyama et al., 2011).

An intriguing finding was the high Myo16b expression in the olfactory bulb in all studied ages, which suggests a continuous Myo16b activity there throughout the lifespan. One explanation for this result could be mouse olfactory bulb neurogenesis, as mice have ongoing neurogenesis in the olfactory bulb (Bergmann et al., 2015). However, postnatal neurogenesis is also present in the hippocampus, both in human and mice (Bergmann et al., 2015), but a similar continuously high Myo16 expression was not observed there. Could myosin XVI play a special role in the olfactory bulb? Could myosin XVIB, for instance, regulate cell division and neurogenesis in the olfactory bulb?

One thing to consider is the unspecific binding of the antibody that could not be totally eliminated in spite of protocol optimization. It seems unlikely that the non-specific bands are only cleavage products or post-translational modifications of myosin XVI as those bands appeared also in knock-out samples. Whether they are different myosin XVI isoforms, different myosins, or something else, remains unanswered. With respect to different isoforms, it is known that rat Myo16b is the principal

isoform expressed in the body, including both the developing and adult brain (Patel et al., 2001). In their study (2001), Patel et al. concluded that Myo16a mRNA expression is minimal compared to Myo16b. However, they also observed minor, assumedly Myo16a bands of around 150 kDa in their blots when using anti-MYO16 directed against the N-terminus and rat tissue samples. The antibody used in the current study was also directed against the N-terminus, suggesting a similar possibility. However, mice do not reportedly have the 150 kDa isoform but instead another isoform of around 200 kDa isoform, which was not observed in the blots. Additional methodological challenges were also faced in this study, from mouse reproduction to preparation of samples, running gel electrophoresis, and quantifying sample loads. Especially the tiny P1 and P11 dissections from the olfactory bulb and hippocampus were challenging to prepare and required adjustments to the protocol. Furthermore, only a small amount of final sample could be prepared. The small volume of samples, together with a limited number of animals, restricted the number of repetitions that could be performed. Myo16 expression was however repeated twice at minimum for each animal, and the results presented here were a consistent finding. Future studied will need to perform more quantitative analyses of Myo16 expression.

Finally, some findings proposed that there might be sex-related or other inter-individual differences in Myo16b expression. The sex of the youngest animals (P1 and P11) was not determined due to methodological issues, however the sex of the older animals was known. This study did not aim to explore sex-related differences, but the possibility that they exist cannot be excluded.

The conclusions drawn from the present results of developmental Myo16b expression pattern are summarized in **Figure 20**. In the future, the cellular distribution of myosin XVI in the examined regions, especially in the olfactory bulb, should be studied in greater detail. Initially, the third aim of this project was to perform immunohistochemistry in mouse brain in order to elucidate whether Myo16 distributes in certain cell types, such as inhibitory interneurons. This would broaden our understanding of the function of myosin XVI in the brain. For example, the olfactory bulb is known to contain inhibitory neurons and excitatory neurons, and their interplay is considered to be essential in odor discrimination (Su et al., 2009).

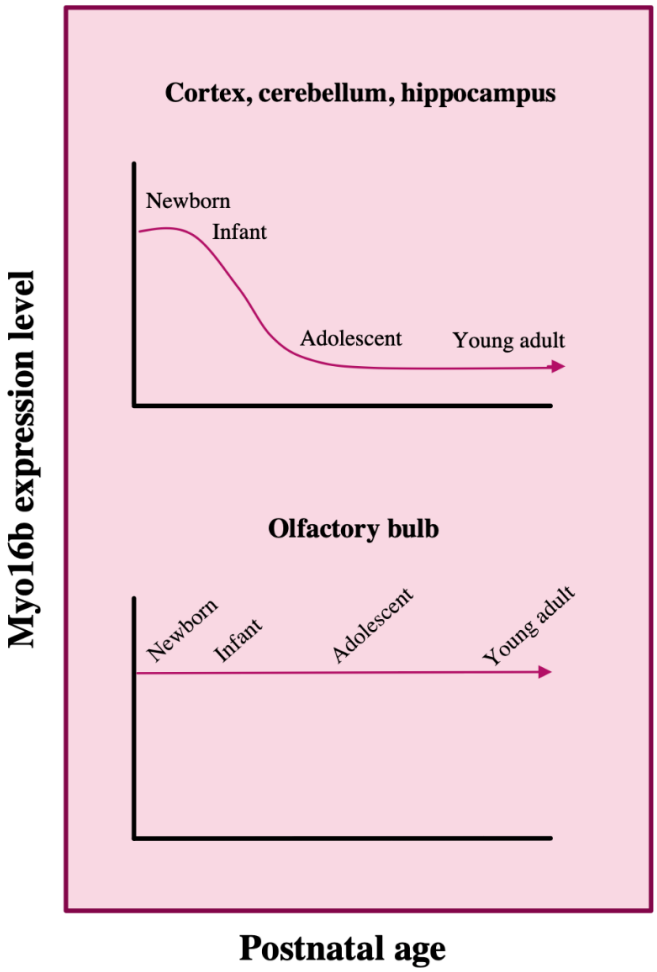

Figure 20. Graphical summary of the conclusions drawn from the developmental Myo16b expression results.

3.3 Linking the findings to ASD and schizophrenia

What could the results of this Thesis mean in the context of the human brain and ASD and schizophrenia? This study suggests that in the non-affected hippocampus, cerebellum, and cortex, there is higher MYO16 expression in early childhood and lower MYO16 expression in adolescence and adulthood. Additionally, this study provides evidence that in the non-affected olfactory bulb, there is quite stable MYO16 expression from early childhood to adolescence and adulthood. The clinical symptoms of ASD usually emerge in early childhood approximately corresponding to mouse age P1–P11, whereas the symptoms of schizophrenia typically manifest themselves in adolescence or in early adulthood approximately corresponding to mouse ages P28 and P56. Some studies have indicated that the expression of MYO16 is lower than normal in the autistic brain and higher than normal in the schizophrenic brain (Liu et al., 2015; Rodriguez-Murillo et al., 2014). Could *MYO16* mutations in ASD lead to reduced MYO16 expression in early childhood and *MYO16* mutations in schizophrenia contrariwise to increased MYO16 expression in adolescence and early adulthood,

causing a differential expression trajectory? Consequently, MYO16 expression could be constantly too low in ASD and constantly too high in schizophrenia.

What could the consequences of altered MYO16 expression be at the cellular level? There is no clear answer as yet, but we can hypothesize. It has been speculated that *MYO16* mutations could contribute to the pathogenesis of ASD via altered dendritic spines (Joensuu et al., 2018). Indeed, disruptions in the PI3K–WRC–Arp2/3 pathway can lead to structurally deficient spines (Hotulainen et al., 2009; Spence et al., 2016). Moreover, F-actin turnover rate may be accelerated in the dendritic spines in the absence of MYO16 (Roesler et al., 2019). Abnormal dendritic spines have been implicated in both ASD and schizophrenia, and it has been hypothesized that their number is too high in the autistic brain and too low in the schizophrenic one (Penzes et al., 2011). The present results propose that one subcellular location of MYO16 is the plasma membrane, supporting the possibility that it participates in the formation of dendritic spines. Perhaps low MYO16 expression leads to too many dendritic spines in ASD and high MYO16 expression leads to too few dendritic spines in schizophrenia.

The symptoms of ASD and schizophrenia are likely not stemming from abnormalities in some specific brain areas but rather from broad neural circuits that extend beyond the boundaries of different brain regions. However, it can be hypothesized that the cognitive and social symptoms may partly be rooted in altered function of MYO16 in the hippocampus, cortex, and cerebellum, and that the olfactory symptoms may, in some extent, be rooted in altered function of MYO16 in the olfactory bulb.

Future studies should also aim to explore the possible sex-related differences in myosin XVI expression in the brain. Interestingly, the prevalence of ASD is higher in males compared to females, with a ratio of approximately 3:1 (Hodges et al., 2020).

An important issue to consider here are developmental differences between human and mouse. Basic neuroanatomy and fundamental developmental processes are highly similar between these two species, but certain aspects are unique to human (Zhao and Bhattacharyya, 2018). For example, human neurodevelopment occurs over a longer time course and is characterized by higher complexity and specific genetic features (Zhao and Bhattacharyya, 2018). Another example is the olfactory bulb. The structure and neuronal count of the olfactory bulb is largely similar between humans and mice (McGann, 2017), but unlike mice humans do not display prominent neurogenesis in the olfactory bulb (Bergmann et al., 2015). Olfactory bulb neurogenesis is very limited or even absent in human adults contrary to most other mammals (Bergmann et al., 2015). This raises a question of whether the

current results – in terms of the olfactory bulb – are fully applicable to human. Nevertheless, the existence of this difference does not necessarily imply a difference in myosin XVI function in the olfactory bulb during early postnatal stages. Despite the fact that certain aspects of human neurodevelopment and neurodevelopmental disorders cannot be fully encapsulated in any other species, animal models still provide important knowledge that can be attributed to human as well.

3.4 Significance of the research

To date, only a handful of articles about myosin XVI have been published. Findings however point to its importance in neurodevelopment and role in some cases of ASD and schizophrenia. Investigating the localization and expression of myosin XVI is therefore a key for obtaining a better insight into how neuronal function and brain development are affected when the expression of myosin XVI is altered.

Neurodevelopmental disorders are extraordinarily complex conditions in terms of pathophysiology, which has considerably complicated diagnostics and development of new treatments. Currently, there is an unmet medical need in both ASD and schizophrenia. Better understanding of the biological underpinnings of these disorders is therefore critical for developing more effective therapies for the affected individuals.

Although ASD and schizophrenia are highly heterogeneous conditions with a multitude of genes having been linked to them, the genes can be clustered into fewer functional entities that can also be differently affected in different individuals (Duda et al., 2018). Pooling the genetic effects and classifying the cases into different subgroups could serve as a basis for development of better treatments. For example, identifying when and understanding how MYO16 is affected might be beneficial for categorizing the cases of ASD and schizophrenia, and further for developing treatments that target similar cases. Most ideally, understanding the developmental expression of proteins involved in ASD and SZ could even enable prevention of the progression of these disorders and outbreak of symptoms.

ASD and schizophrenia are two common, persistent, and debilitating conditions that have long remained without exact explanations and are still stigmatized in the society. Therefore, understanding the biology of ASD and schizophrenia better and moving the science forward around them is important for the affected individuals, for their relatives, as well as for the society as a whole.

4 Materials and methods

4.1 Fluorescence staining

4.1.1 Cell culture

The human bone osteosarcoma epithelial (U2OS) cell line was selected as a model for studying the subcellular localization of myosin XVI for several reasons. U2OS cells exhibit a pronounced actin cytoskeleton with clear F-actin structures, and the normal cytoskeletal organization of these cells is also well known in the group. U2OS cells are relatively flat and have small enough nuclei to distinguish cytoplasmic structures. In addition, U2OS were more reliably available than primary cells, such as neurons. Furthermore, U2OS cells are more durable, transfectable, and ethically justified than primary cells. According to the Human Protein Atlas, U2OS cells express MYO16 mRNA, indicating that they are endogenously expressing the protein.

U2OS cells were obtained as a gift from another research group and stored at -140°C. Cell culture was created by quickly thawing the cells at 37°C and suspending them in 5 ml of pre-warmed Dulbecco's Modified Eagle's Medium (DMEM) – high glucose (#D6429, Sigma-Aldrich) supplemented with 10% fetal bovine serum, 1% L-glutamine and 0.5% penicillin–streptomycin (i.e., growth medium). The cells were centrifuged (900 g, 4 min) and the resulting cell pellet resuspended in 10 ml of fresh growth medium. The cells were cultured in standard conditions (37°C, 5% CO_2) on standards cell culture dishes (100 x 20 mm, #664 160, Greiner Bio-One) and passaged when they were around 70% confluent. Passaging was performed by first washing the cells once with phosphate-buffered saline (PBS) and adding 1 ml of Trypsin–EDTA solution (#T3924, Sigma-Aldrich). Then the cells were incubated in standard conditions (5 min), mixed with 8 ml of fresh growth medium, and transferred to a new dish with fresh growth medium in a ratio of about 1:5.

4.1.2 Plasmid production

Three different plasmids, tagged with enhanced green fluorescent protein (EGFP), were used in transfection of U2OS cells; pEGFP-*MYO16B* (human, full-length 1858 aa isoform) and pEGFP-*Myo16b* (rat, full-length 1912 aa isoform) for examining the subcellular localization of myosin XVIB, and pEGFP-N1 for transfection control. Rat pEGFP-*Myo16b* plasmids was produced by the author of this Thesis. Human pEGFP-*MYO16B* and pEGFP-N1 plasmids were produced earlier by other group members, similarly than the rat pEGFP-*Myo16b* discussed below.

Production of rat plasmid DNA was performed using DH5α competent *Escherichia coli* cells and plasmid vectors containing genes for EGFP, kanamycin resistance, and full-length rat Myo16 (20 ng/µl pEGFP-C3-*Myo16b*). Bacterial transformation was initiated by thawing the bacteria and the plasmid vectors on ice. Then the plasmids were mixed with the cells 1:20 in a sterile tube. The resulting solution was cooled down on ice (20 min), followed by a quick heat shock (40 sec, at 42°C) and subsequent cooling on ice (5 min). 500 µl of S.O.C. Medium (#15544-034, Invitrogen) was added to the solution and the bacteria were cultured in an incubator (1 h, shaking 250 rpm, at 37°C). 200 µl of the culture was placed on a kanamycin plate, air-dried, and incubated again upside-down (18 h, at 37°C). One of the kanamycin-resistant DH5α colonies was picked and mixed with 4 ml of Lysogeny broth medium (#T00053, Huslab) containing 25 µg/ml kanamycin. The bacteria were cultured (5 h, shaking 225 rpm, at 37°C), mixed with 200 ml of Lysogeny broth medium containing 50 µg/ml kanamycin, and cultured once again (18 h, 225 rpm, at 37°C). Plasmid DNA was purified using the maxiprep method and QIAfilter Plasmid Maxi Kit (25) (#12263, Qiagen), and proceeding as instructed in the Qiagen QIAfilter Plasmid Purification Handbook: www.qiagen.com/HB-1169. First, the transformed bacteria were centrifuged (30 min, 4600 x *g*, at 4°C) and the resulting pellets resuspended in Buffer P1. Buffer P2 was added and the lysates incubated (5 min, at RT), after which Buffer P3 was added and the lysates poured into capped QIAfilter Cartridge tubes where the lysates were kept for 10 min. Then the tubes were uncapped and placed on equilibrated QIAGEN-tip filter tubes through which the lysates were filtered with a plunger. The filter tubes were washed twice with Buffer QC and plasmid DNA eluted to new tubes with pre-warmed Buffer QF. Plasmid DNA was precipitated by adding 10.5 ml of isopropanol, centrifuging (1 h, 4600 x *g*, at 4°C), diluting the pellets in 5 ml of 70% ethanol, and centrifuging again (30 min, 4600 x *g*, at 4°C). The pellets were air-dried and dissolved in 200 µl of Tris-EDTA buffer (pH 8.0). Finally, concentration of the plasmid DNA was measured using NanoDrop™ One instrument (Thermo Scientific). Final concentration of 1.0 µg/µl was obtained by mixing the plasmid DNA solution with Tris-EDTA buffer. The plasmids were stored at -20°C.

4.1.3 Lipofectamine transfection

The U2OS cells were counted and plated in smaller culture plate wells the day before transfection. Cover glasses (Ø 13 mm, 0.16 mm, #631-0150, WWR), first stored in 70% ethanol, were placed in 24-well culture plates (#3524, Corning Costar®) and disinfected in ultraviolet light for 15 min. The cells, about 70% confluent, were counted by gently mixing trypsinized cells with fresh growth

medium and pipetting the cells to a counting slide (#1450015, Bio-Rad). Cell density was counted using TC20™ automated cell counter (#1450102, Bio-Rad). Based on the average result of six repeated measurements a final concentration of 40 000 cells/ml (20 000 cells per well) was obtained by blending cells and fresh growth medium up to the required volume. The culture plate wells were washed twice with PBS, the cells added and then cultured in standards conditions for around 18 h. Prior to transfection, the cells were washed with PBS and the normal growth medium was changed to medium without antibiotics, followed by 1 h incubation in standards conditions. First, Lipofectamine® 2000 Reagent (#11668-019, Thermo Scientific) was diluted in DMEM (2 ul Lipofectamine + 50 ul DMEM per well) and similarly each plasmid DNA (human pEGFP-*MYO16B*, rat pEGFP-*Myo16b*, pEGFP-N1) was diluted in DMEM (0.8 ug DNA + 50 ul DMEM per well). These solutions were incubated separately for 5 min (at RT) before mixing the Lipofectamine solution with each plasmid DNA solution (1:1). The resulting transfection mixes were again incubated (25 min, at RT), after which 100 µl of transfection mix was pipetted dropwise to each well, excluding untransfected controls that were otherwise treated similarly to transfected cells. Then the cells were incubated in standard conditions for 5 h. Transfection was completed by washing the cells twice with PBS and changing to the normal growth medium, and the cells were let to grow in standard conditions for around 18 h. The cells were washed twice with PBS and finally fixed by adding 250 µl of 4% paraformaldehyde in PBS per well, incubating (20 min, at 37°C), and washing again twice with PBS. The cells were stored in PBS at 4°C, with parafilm around, until staining.

The treatment of untransfected U2OS cells, intended for studying endogenous expression of MYO16, was similar to transfected cells, excluding transfection. The cells were similarly plated in 24-well plates on coverslips, 40 000 cells/ml (20 000 cells per well) and cultured in standard conditions for around 18 h before fixation and storing.

4.1.4 Staining

Transfected U2OS cells were stained with Alexa Fluor® 594 phalloidin (#A12381, Invitrogen; F-actin marker) and PureBlu™ DAPI (#1351303, Bio-Rad; DNA marker). First the cells were washed with PBS, permeabilized with 300 µl of 0.5% Triton X-100 in PBS per well (7 min), washed again with PBS, and blocked with 300 µl of 3% normal donkey serum (#S2170-100, Biowest) with 0.5% bovine serum albumin (BSA) in PBS per well (30 min or longer). Then the cells were incubated with 25 µl of Alexa Fluor 594 phalloidin (1:400 in the blocking solution) (1h, at RT, in darkness). Next, the cells were incubated with 25 µl of DAPI (1:100 in 0.1% Triton X-100 in PBS) (20 min, at RT, in

darkness). The cells were washed with 0.2% BSA in PBS (3 x 10 min, 150 rpm, in darkness) and then the coverslips were dipped in mQH_2O, gently dried, and mounted on imaging slides (#12372098, Thermo Scientific) with 15 µl of Shandon™ Immu-Mount™ mounting medium (#9990402, Thermo Scientific). The slides were kept at RT overnight before storing them at 4°C.

Untranfected U2OS cells were stained with anti-MYO16 antibodies, Alexa Fluor 594 phalloidin, and DAPI. Four different anti-MYO16 antibodies were tested: rabbit polyclonal anti-MYO16 from MyBioSource (#MBS9609973), rabbit polyclonal anti-MYO16 from Proteintech (#25104-1-AP), rabbit polyclonal anti-MYO16 from Biorbyt (#orb629102), and anti-MYO16 obtained as a gift from another research group (described in Cameron et al., 2007). Permeabilization and blocking of the cells were carried out as with transfected cells. The cells were then incubated with 25 µl of anti-MYO16 (MyBioSource, Proteintech, and Biorbyt anti-MYO16: 1:200 in the blocking solution; Cameron et al.'s anti-MYO16: 1:150 in the blocking solution) (1.5 h, at RT). Then the cells were washed with 0.2% BSA in PBS with gently shaking (3 x 10 min, 150 rpm) before incubation with 25 µl of Alexa Fluor® 488 donkey anti-rabbit lgG antibody (#A21206, Invitrogen; secondary antibody) and Alexa Fluor 594 phalloidin (1:400 and 1:400 in the blocking solution) (1 h, at RT, in darkness), and subsequent incubation with 25 µl of DAPI (1:100 in 0.1% Triton X-100 in PBS) (20 min, at RT, in darkness). Finally, the cells were washed with 0.2% BSA in PBS (3 x 10 min, 150 rpm, in darkness), and mounted and stored as the transfected cells.

Some of the transfected U2OS cells were also stained with anti-MYO16, Alexa Fluor 594 phalloidin, and DAPI to examine whether the antibodies recognize overexpression. This staining was otherwise similar to staining of untransfected cells, but Alexa Fluor 488 was replaced with Alexa Fluor® 647 goat anti-rabbit lgG antibody (#A21244, Invitrogen). Additionally, some of the transfected cells were stained with mouse monoclonal anti-PDI antibody (1D3) (#SPA-891, Assay Designs/Stressgen; ER marker), Alexa Fluor 594 phalloidin, and DAPI, or mouse monoclonal anti-γ-tubulin (#T6557, Sigma-Aldrich; microtubule organizing center (MTOC) marker), Alexa Fluor 594 phalloidin, and DAPI. These stainings were otherwise similar to staining of untransfected cells, but anti-MYO16 and Alexa Fluor 488 were replaced with anti-PDI (1:200 in the blocking solution) or anti-γ-tubulin (1:5000 in the blocking solution) and Alexa Fluor® 647 donkey anti-mouse lgG antibody (#A31571, Invitrogen; 1:400 in the blocking solution).

Transfection controls were EGFP-N1-expressing U2OS cells (positive transfection control) and untransfected U2OS cells (non-treated control). Secondary antibody control was used for the cells stained with either anti-MYO16, anti-PDI, or anti-γ-tubulin (Alexa Fluor 488 or Alexa Fluor 647).

4.1.5 Microscopy

U2OS cells were imaged at Biomedicum Bioimaging Unit, using Zeiss Axio Imager 2 epifluorescence microscope with Hamamatsu Orca Flash 4.0 LT camera and Zen Blue software. 63x oil and 100x oil objectives were used to reach good resolution. The images were processed using Fiji ImageJ software (version 2.1.0/1.53c).

4.2 Western blotting

4.2.1 Mice and genotyping

The mouse cell line was obtained as a generous gift from Wolfgang Wagner and his colleagues (described in Roesler et al., 2019). The wild-type mice were C57BL/6J (B6) strain, the *Myo16* knock-out model B6-*Myo16*^{em3}/J (*Myo16*-KO-43L). Animals were housed 2–3 mice per cage in a controlled environment (temperature 21 ± 1°C, humidity 50 ± 10%, light period 07:00 AM to 7:00 PM) and supplied with food and water *ad libitum*.

Genotyping was performed to select wild-type (*Myo16*$^{+/+}$) and knock-out (*Myo16*$^{-/-}$) mice for western blotting. Thermo Scientific Phire Tissue Direct PCR Master Mix (#F170S) kit was used for genotyping the mice. P1 mice were genotyped using tail samples and the older animals using ear samples. First, Dilution Buffer and DNARelease Additive were mixed (1:40) and 20 µl of the resulting mix added to each tissue sample. DNA was extracted using C1000 Touch™ Thermal Cycler (Bio-Rad) (program: 2 min at RT, 2 min at 98°C, stand by 4°C). Phire Tissue direct PCR Master Mix (2X), mQH_2O and primers (*Myo16* forward and reverse; obtained from Wolfgang Wagner's group) were mixed with DNA extraction (8:8:1:1:2) and the DNA amplified (program: initial denaturation, 98°C – 120 sec, denaturation 98°C – 10 sec, annealing 68°C – 20 sec, extension 72°C – 25 sec x35, final extension 72°C – 300 sec, stand by 4°C). 18 µl samples and 10 µl GeneRuler 100 bp DNA Ladder was loaded per well. Agarose gel (1.5% agarose in Tris-acetate-EDTA buffer with 6 µl of Midori Green Advance DNA stain [#MG04, Nippon Genetics]) electrophoresis was run (30 min, 60 V) and the bands imaged using ChemiDoc™ Touch Imaging System (Bio-Rad) (**Figure 21**). Both

positive (+/+, -/-, +/-) and negative (mQH_2O) controls were used to confirm the results. Myo16 wild-type and Myo16 knock-out bands were 400 bp and 150 bp, respectively.

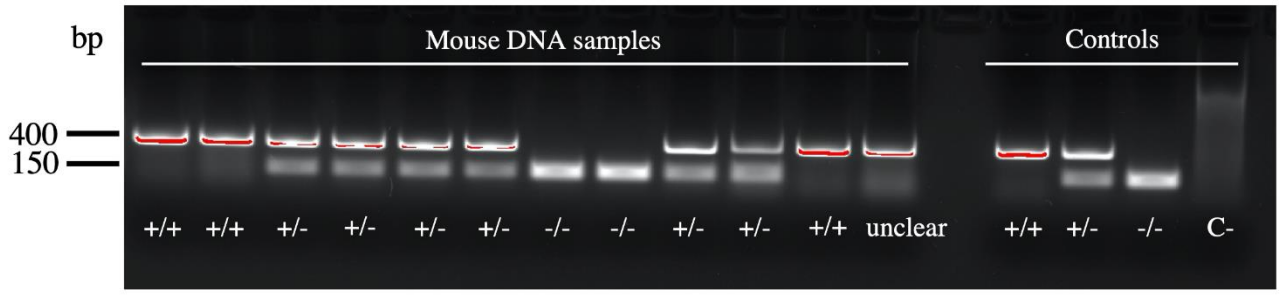

Figure 21. One of the mouse genotyping gels. Wild-type (*Myo16*$^{+/+}$) mice have a 400 bp band, knock-out (*Myo16*$^{-/-}$) mice have a 150 bp band, and heterozygous (*Myo16*$^{+/-}$) mice have both 150 bp and 400 bp bands. C-, negative control (mQH_2O only). Samples: 18 µl, DNA ladder: 10 µl.

4.2.2 Preparation and western blotting of mouse brain homogenates

Mice were sacrificed under Mebunat anesthesia. For P11, P28, P56 and ~P250, the other brain hemisphere was dissected to the olfactory bulb, hippocampus, cerebellum and cortex. For P1, both hemispheres were dissected in order to have the minimum required amount of tissue for sample preparation. The samples were stored without liquid at -80°C. These steps were performed by another group member.

Brain samples were thawed and handled on ice. Radioimmunoprecipitation assay buffer (150 mM NaCl, 1.0% NP-40, 0.5% Sodium deoxycholate, 50 mM Trizma base, no SDS; pH 8.0) containing 10% Complete (protease inhibitor cocktail tablets, dissolved in mQH_2O, #04693116001, Roche) and 10% PhosSTOP (phosphatase inhibitor cocktail tablets, dissolved in mQH_2O, #04906837001, Roche) was added to the samples, ranging from 50–400 µl according to the estimated volume of each tissue sample. Samples containing 300 µl or more of the lysis buffer (~P250: all, P56: all, P28: cortex) were transferred into 2 ml soft tissue homogenizing tubes with 1.4 mm ceramic beads (#10032-358, Omni International) and homogenized using Bead Ruptor Elite Bead Mill Homogenizer (Omni International) with the program for brain tissue (4.85 m/s, 20 sec). After this the homogenates were again transferred to new Eppendorf tubes. Samples containing 80–300 µl lysis buffer (P28: olfactory bulb, hippocampus, cerebellum; P11: hippocampus, cerebellum, cortex; P1: cerebellum, cortex) were homogenized manually using Dremel® 3000 multi-tool (3000-15) with a sterilized attachment for homogenization (3 x 8 sec at RT, on ice in between). Samples with less than 80 µl lysis buffer (P11; olfactory bulb; P1: olfactory bulb, hippocampus) were disrupted manually with a needle and by quick

vortexing. The samples were centrifuged (15 min, 14 000 rpm, at 4°C), followed by collection of supernatants to new Eppendorf tubes, adding 1% SDS, and new centrifugation (14 000 rpm, 20 min, at 4°C). The resulting supernatants were transferred to new Eppendorf tubes prior to protein concentration measurement. Protein concentrations were determined using BCA Protein Assay Kit (#23227, Thermo Scientific). Blank (mQH_2O) standards, BSA standards, and tissue samples were diluted in mQH_2O (1:9) in 96-well microplates and incubated with BCA Reagent mix (30 min, at 37°C). Absorbances were measured using EnSpire® MultiMode Plate Reader (PerkinElmer) and protein concentrations calculated from triplicate average values. The final samples for western blotting contained either 1.0 mg/ml (P11, P28, P56, ~P250) or 0.50 mg/ml (P1) protein, depending on the initial concentrations, in mQH_2O and 1x Laemmli buffer (from 4x Laemmli Sample Buffer, #161-0747, Bio-Rad). The samples were boiled (5 min, at 100°C) and stored at 4°C until western blotting.

7.5% stain-free polyacrylamide gels (TGX Stain-Free™ FastCast™ Acrylamide kit, #161-0181, Bio-Rad) were cast for gel electrophoresis. 10–20 µg protein per well was loaded for each sample, with 10 µl stained standard proteins (Precision Plus Protein™ All Blue Standards, #1610373, Bio-Rad) and unstained standard proteins (Precision Plus Protein™ Unstained Protein Standards, #1610363, Bio-Rad). The gels were run in Tris-Glycine-SDS buffer on ice, at 200 V for 1 h 45 min and, unfortunately, standard proteins below 75 kDa were run out of the gel. This was done because the Proteintech anti-MYO16 used in western blotting appeared to bind to several proteins of around the same size as Myo16, and this unspecific binding interfered with the detection as the unspecific bands overlapped with Myo16 bands. When the gel was run longer, the unspecific bands were more separated from Myo16 bands which were then more easily distinguished.

Gel electrophoresis was followed by the steps described in Trans-Blot Turbo Transfer System Instruction Manual: https://www.bio-rad.com/webroot/web/pdf/lsr/literature/10020688.pdf. First, the gels were activated using ChemiDoc™ Touch instrument. Protein transfer was performed using Trans-Blot® Turbo™ RTA Transfer Kit, LF PVDF (#1704274, Bio-Rad) and Trans-Blot® Turbo™ Transfer System (#1704150, Bio-Rad). Polyvinylidene difluoride membranes were first immersed in 95% ethanol. Then ion reservoir stacks and the membranes were soaked in transfer buffer (with 1x Transfer Buffer and 20% ethanol in mQH_2O) for a few minutes and assembled into a transfer pack. Protein transfer was run using Trans-Blot® Turbo (Bio-Rad) and the program for high molecular weight proteins (25 V for 10 min). After transfer, the membranes were soaked first in mQH_2O, then in 70% ethanol, and activated using ChemiDoc™ Touch. The membranes were blocked in 5% milk

in Tris-buffered saline with 0.1% Tween® 20 (TBST) (1 h, shaking, at RT) and incubated with the primary antibody (1:1000 Proteintech anti-MYO16 (#25104-1-AP) in 5% milk and TBST, with 0.02% sodium azide) (around 18 h, shaking, at 4°C). The membranes were washed in TBST (5 x 6 min, shaking, at RT), incubated with the secondary antibody (1:10 000 HRP-conjugated mouse anti-rabbit lgG antibody [#211-032-171, Jackson Immunoresearch]) in 5% milk and TBST) (1 h, shaking, at RT), washed again in TBST (3 x 10 min, shaking, at RT), and finally incubated in SuperSignal™ West Pico PLUS Chemiluminescent Substrate (#34577, Thermo Scientific) mix (2.5 min, gentle manual shaking). Finally, Myo16 was visualized using chemiluminescence detection in ChemiDoc™Touch. The images were analyzed with ImageJ software (version 2.1.0/1.53c) and Excel (version 16.30).

In addition to Proteintech anti-MYO16, MyBioSource anti-MYO16 (#MBS9609973) was also tested for western blotting. The selection of a suitable antibody for western blotting was performed by incubating the same membrane first with one antibody, then stripping the membrane, and then incubating with the other antibody, similarly to the previous one. The membranes were stripped by washing them in TBST (10 min, shaking, at RT), incubating in glycine buffer (0.1 M, pH 2.0) (shaking, 1 h), and then washing again in TBST (3 x 10 min, shaking, at RT).

4.2.3 Preparation and western blotting of U2OS cell lysates

Western blotting was also performed to U2OS cell lysates in order to verify that MYO16 is endogenously expressed in U2OS cells and also to confirm overexpression. For this, transfected cells were not fixed but instead washed twice with PBS. 150 µl of 1x Laemmli to was added to human EGFP-MYO16, rat EGFP-Myo16, EGFP-N1 control, and untransfected control wells, and the cells were detached with a scratcher. The cells of four consecutive wells were pooled into one, transferred to Eppendorf tubes, and boiled (10 min, at 100°C). 25 µl of each cell lysate was used in western blotting. Western blotting was performed similarly than with mouse tissue samples, except for incubation with anti-GFP antibody (1:1000 rabbit polyclonal anti-GFP (#A-11122, Invitrogen) in 5% milk and TBST, with 0.02% sodium azide), which was followed by incubation with anti-MYO16 and stripping.

5 Ethical issues

Instead of using primary cells derived from animals, U2OS cell line, initially derived from human, were used in subcellular localization experiments. In order to study myosin XVI localization in the brain at different points in development, animals were needed since the brains cannot be examined by other means. Mice were selected as a model because the mouse brain is considered relatively similar to the human brain in respect to the studied regions.

All experiments were carried out in accordance with the guidelines laid down with the European Communities Council directive of 2010/63/EU and were approved by the County Administrative Board of Southern Finland.

Myo16 knock-out mice were under the University of Helsinki license KEK19-035 (MYO16 in psychiatric diseases).

6 Acknowledgements

I want to thank my Supervisors for their encouragement and firm belief in my abilities – special thanks to Jolanta Lundgren for the patient teaching of lab work and to Rimante Minkevicience for her work with mice. I also want to express my gratitude to Pirta Hotulainen for the opportunity to complete my Thesis work in the group of Cellular Neuroscience, as well as for the critical reading of this Thesis. I am also very grateful for all the other people at Minerva Institute for helping and creating a warm work atmosphere, as well as for the staff of Biomedicum Imaging Unit for the advice with microscopy. At the University of Turku, I want to thank especially Ullamari Pesonen who was my third Supervisor. Finally, the support from my family and friends – from my boyfriend Riku in particular – has been invaluable.

This work was supported by the Päivikki and Sakari Sohlberg Foundation under Grant “Muutokset hajuaistissa on yhteinen nimittäjä autismikirjon häiriölle ja skitsofrenialle – selviääkö hajukäämistä neuropsykiatristen sairauksien biologiset syyt?” and Minerva Foundation.

7 Abbreviations list

ACOT9	Acyl-CoA thioesterase 9
Arp2/3	actin-related protein 2/3
ASD	autism spectrum disorder
DMEM	Dulbecco's Modified Eagle's Medium
F-actin	filamentous actin
GRAF1	GTPase Regulator Associated with Focal Adhesion Kinase-1
MTOC	microtubule organizing center
NES	nuclear export signal
NHM	NYAP homology motif
NLS	nuclear localization signal
NYAP	neuronal tyrosine-phosphorylated adaptor for PI3K
PI3K	phosphoinositide 3-kinase
PPIc	protein phosphatase type 1 catalytic subunit
SNP	single nucleotide polymorphism
TBST	Tris-buffered saline with 0.1% Tween 20
U2OS	human bone osteosarcoma epithelial cell line
WAVE1	Wiskott–Aldrich syndrome protein/verprolin homologue 1
WRC	WAVE regulatory complex

8 References

Abrahams, B.S., and D.H. Geschwind. 2008. Advances in autism genetics: in the threshold of a new neurobiology. *Nat Rev Genet.* 9(5):341-355. doi:10.1038/nrg2346.

Allen Brain Atlas 2020: Myosin XVI. [online] Available at: <https://mouse.brain-map.org/gene/show/89217> [Accessed September 12, 2020].

Andersen, S.L. 2003. Trajectories of brain development: point of vulnerability or window of opportunity? *Neurosci Biobehav Rev*. 27(1-2):3-18. doi:10.1016/s0149-7634(03)00005-8.

Andreasen, N.C., and R. Pierson. 2008. The role of the cerebellum in schizophrenia. *Biol psychiatry*. *64*(2):81–88. doi:10.1016/j.biopsych.2008.01.003.

Ashwin, C., E. Chapman, J. Howells, D. Rhydderch, I. Walker, and S. Baron-Cohen. 2014. Enhanced olfactory sensitivity in autism spectrum conditions. *Mol Autism* 5:53. doi: 10.1186/2040-2392-5-53.

Baarlink, C., M. Plessner, A. Sherrard, K. Morita, S. Misu, D. Virant, E. Kleinschnitz, R. Harniman, D. Alibhai, S. Baumeister, K. Miyamoto, U. Endesfelder, A. Kaidi, and R. Grosse. 2017. A transient pool of nuclear F-actin at mitotic exit controls chromatin organization. *Nat Cell Biol*.19:1389–1399. doi:10.1038/ncb3641.

Bailey, A., A. Le Couteur, I. Gottesman, P. Bolton, E. Simonoff, E. Yuzda, M. Rutter. 1995. Autism as a strongly genetic disorder: Evidence from a British twin study. *Psychol Med*, 25: 63–77. doi:10.1017/s0033291700028099.

Bennetto, L., E.S. Kuschner, and S.L. Hyman. 2007. Olfaction and taste processing in autism. *Biol psychiatry*, 62(9):1015–1021. doi:10.1016/j.biopsych.2007.04.019.

Bergmann, O., K.L. Spalding, and J. Frisén. 2015. Adult Neurogenesis in Humans. *Cold Spring Harb Perspect Biol*. *7*(7), a018994. doi:10.1101/cshperspect.a018994.

Bourne, J.N., and K.M. Harris. 2008. Balancing structure and function at hippocampal dendritic spines. *Annu Rev Neurosci.* 31:47–67. doi:10.1146/ annurev.neuro.31.060407.125646.

Bugyi, B., and A. Kengyel. 2020. Myosin XVI. *Adv Exp Med Biol*. 1239:405-419. doi:10.1007/978-3-030-38062-5_18. In Myosins - A Superfamily of Molecular Motor*s.* 2nd ed., pp. 405-419. Boston, USA: *Springer.* Edited by L. Coluccio,

Cameron, R.S., C. Liu, A.S. Mixon, J.P. Pihkala, R.J. Rahn, and P.L. Cameron. 2007. Myosin 16b: The COOH-tail Region Directs Localization to the Nucleus and Overexpression Delays S-Phase Progression. *Cell Motil Cytoskeleton*. 64:19–48. doi:10.1002/cm.20162.

Carlsson, A.E. 2010. Actin dynamics: from nanoscale to microscale. *Annu Rev Biophys*. 39:91–110. doi:10.1146/annurev.biophys.093008.131207.

Chang, S.C., D.L. Pauls, C. Lange, R. Sasanfar, and S.L. Santangelo. 2013. Sex-specific association of a common variant of the XG gene with autism spectrum disorders. *Am. J. Med. Genet. Part. B Neuropsychiatr. Genet.* 162(7): 742–750. doi:10.1002/ajmg.b.32165.

Chen, J.A., O. Peñagarikano, T.G. Belgard, V. Swarup, and D.H. Geschwind. 2015. The Emerging Picture of Autism Spectrum Disorder: Genetics and Pathology. *Annu Rev Pathol Mech Dis*. 10:111–44. doi: 10.1146/annurev-pathol-012414-040405

Connolly, J.J., J.T. Glessner, H. Hakonarson. 2013. A genome-wide association study of autism incorporating autism diagnostic interview-revised, autism diagnostic observation schedule, and social responsiveness scale. *Child Dev.* 84 17–33. 10.1111/j.1467-8624.2012.01838.x

Cook, E.H. Jr., and S.W. Scherer. 2008. Copy-number variations associated with neuropsychiatric conditions. *Nature.* 455:919–923. doi:10.1038/nature07458.

Cohen, P.T. 2002. Protein phosphatase 1 – targeted in many directions. *J Cell Sci*. 115:241-256.

Dacks, J.B., A.A. Peden, and M.C. Field. 2009. Evolution of specificity in the eukaryotic endomembrane system. *Int J Biochem Cell Biol*. 41(2):330-340. doi:10.1016/j.biocel.2008.08.041.

DECIPHER database: MYO16 [online] Available at: <https://www.deciphergenomics.org/search/patients/results?q=myo16> [Accessed April, 2021].

DeFilippis, M., and K.D. Wagner. 2016. Treatment of Autism Spectrum Disorder in Children and Adolescents. *Psychopharmacol Bull*. 46(2):18–41.

de Lanerolle, P. 2012. Nuclear actin and myosins at a glance. *J Cell Sci*. 125(Pt 21):4945–4949. doi:10.1242/jcs.099754.

Di Ventura, B., and B. Kuhlman. 2016. Go in! Go out! Inducible control of nuclear localization. *Curr Opin Chem Biol. 34*:62–71. doi:10.1016/j.cbpa.2016.06.009.

Dominguez, R., and K.C. Holmes. 2011. Actin structure and function. *Annu Rev Biophys*. 40:169-186. doi:10.1146/annurev-biophys-042910-155359.

Duda, M., H. Zhang, H. Li, D.P. Wall, M. Burmeister, and Y. Guan. 2018. Brain-specific functional relationship networks inform autism spectrum disorder gene prediction. *Transl Psychiatry*. 8:56. doi:10.1038/s41398-018-0098-6.

Espreafico, E.M., D.E. Coling, V. Tsakraklides, K. Krogh, J.S. Wolenski, G. Kalinec, and B. Kachar. 1998. Localization of myosin-V in the centrosome. *PNAS.* 95(15):8636-8641. doi:10.1073/pnas.95.15.8636.

Fibiger, H.C. 2012. Psychiatry, the pharmaceutical industry, and the road to better therapeutics. *Schizophr Bull*. 38(4):649–650. doi:10.1093/schbul/sbs073.

Flynn, K.C. 2013. The cytoskeleton and neurite initiation. *Bioarchitecture*. 3(4):86–109. doi:10.4161/bioa.26259.

Folstein, S.E., and J. Piven. 1991. Etiology of autism: genetic influences. *Pediatrics*. 87:767–773.

Forrest, M.P., E. Parnell, and P Penzes. 2018. Dendritic structural plasticity and neuropsychiatric disease. *Nat Rev.* 19:215-234. doi:10.1038/nrn.2018.16.

Foth B.J., M.C. Goedecke, and D. Soldati. 2006. New insights into myosin evolution and classification. *Proc Natl Acad Sci U S A*. 7;103(10):3681-6. doi:10.1073/pnas.0506307103.

Friedman, J., S. Adam, L. Arbour, L. Armstrong, A. Baross, P. Birch, C. Boerkoel, S. Chan, D.Chai, A.D. Delaney, S. Flibotte, W.T. Gibson, S. Langlois, E. Lemyre, H.I. Li, P. MacLeod, J. Mathers, J.L. Michaud, B.C. McGillivray, M.S. Patel, H. Qian, G.A. Rouleau, M.I. Van Allen, S. Yong, F.R. Zahir, P. Eydoux, and M.A. Marra. 2009. Detection of pathogenic copy number variants in children with idiopathic intellectual disability using 500 K SNP array genomic hybridization. *BMC Genomics*. 10:526. doi:10.1186/1471-2164-10-526.

Gao, R., and P. Penzes. 2015. Common Mechanisms of Excitatory and Inhibitory Imbalance in Scizophrenia and Autism Spectrum Disorders. *Curr Mol Med*. 15(2):146–167.

Gauthier. J., T.J. Siddiqui, P. Huashan, D. Yokomaku, F.F. Hamdan, N. Champagne, M. Lapointe, D. Spiegelman, A. Noreau, R.G. Lafrenière, F. Fathalli, R. Joober, M.O. Krebs, L.E. DeLisi, L. Mottron, E. Fombonne, J.L. Michaud, P. Drapeau, S. Carbonetto, A.M. Craig, and G.A. Rouleau. 2011. Truncating mutations in NRXN2 and NRXN1 in autism spectrum disorders and schizophrenia. *Hum Genet*. 130(4):563-73. doi:10.1007/s00439-011-0975-z.

Goley, E., and W. Welch. 2006. The ARP2/3 complex: an actin nucleator comes of age. *Nat Rev Mol Cell Biol*. **7:**713–726. doi:10.1038/nrm2026.

Harrison, P.J. 1999. The neuropathology of schizophrenia: A critical review of the data and their interpretation. *Brain*. 122(4):593–624. doi:10.1093/brain/122.4.593.

Hartman, M.A., and J.A. Spudich. 2012. The myosin superfamily at a glance. *J Cell Sci*. 125(7):1627-1632. doi:10.1242/jcs.094300.

Hazen, E.P., L. Jennifer J.L. Stornelli, J.A. O'Rourke, PhD, K. Koesterer, and C.J. McDougle. 2014. Sensory Symptoms in Autism Spectrum Disorders. *Harv Rev Psychiatry*. 22(2):112-124. doi:10.1097/01.HRP.0000445143.08773.58.

Hering, H., and M. Sheng. 2001. Dentritic spines : structure, dynamics and regulation. *Nat Rev Neurosci.* 2:880–888 doi:10.1038/35104061.

Hikosaka, O. 2010. The habenula: from stress evasion to value-based decision-making. Nat Rev Neurosci. 11:503–513. doi:10.1038/nrn2866.

Hodges, H., C. Fealko, and N. Soares. 2020. Autism spectrum disorder: definition, epidemiology, causes, and clinical evaluation. *Transl Pediatr*. 9(Suppl 1):S55–S65. doi:10.21037/tp.2019.09.09

Hotulainen P., and C.C. Hoogenraad. 2010. Actin in dendritic spines: connecting dynamics to function. *J Cell Biol.* 189: 619–629. doi:10.1083/jcb.201003008.

Hotulainen, P., O. Llano, S. Smirnov, K. Tanhuanpää, J. Faix, C. Rivera, and P. Lappalainen. 2009. Defining mechanisms of actin polymerization and depolymerization during dendritic spine morphogenesis. *J Cell Biol*. 20;185(2):323-39. doi:10.1083/jcb.200809046.

Hu, V.W., and M.E. Steinberg. 2009. Novel clustering of items from the Autism Diagnostic Interview-Revised to define phenotypes within autism spectrum disorders. *Autism Res*. 2:67–77. doi:10.1002/aur.72.

Hubert T., J. Vandekerckhove, and J. Gettemans. 2011. Actin and Arp2/3 localize at the centrosome of interphase cells. *Biochem Biophys Res Commun*. 7(1):153-8.doi:10.1016/j.bbrc.2010.11.084.

Javitt, D.C. 2009. Sensory processing in schizophrenia: neither simple nor intact. *Schizophr Bull. 35*(6):1059–1064. doi:10.1093/schbul/sbp110.

Joensuu, M., V. Lanoue, P. Hotulainen. 2018. Dendritic spine actin cytoskeleton in autism spectrum disorder. *Prog Neuropsychopharmacol Biol Psychiatry*. 84:362-381. doi:10.1016/j.pnpbp.2017.08.023.

Kengyel, A., B. Bécsi, Z. Kónya, J.R. Sellers, F. Erdodi, and M. Nyitrai. 2015. Ankyrin domain of myosin 16 influences motor function and decreases protein phosphatase catalytic activity. *Eur Biophys J*. 44:207–218 doi:10.1007/s00249-015-1015-z.

Kennedy, D.P., and R. Adolphs. 2012. The social brain in psychiatric and neurological disorders. *Trends Cogn Sci*. 16(11):559-572. doi:10.1016/j.tics.2012.09.006

Kenny, E.M., P. Cormican, S. Furlong, E. Heron, G. Kenny, C. Fahey, E. Kelleher, D. Tropea, R. Anney, A.P. Corvin, G. Donohoe, L. Gallagher, M. Gill, and D.W. Morris. 2014. Excess of rare novel loss-of-function variants in synaptic genes in schizophrenia and autism spectrum disorders. *Mol. Psychiatry.* 19 872–879. 10.1038/mp.2013.127

Krendel, M., and M.S. Mooseker. 2005. Myosins: tails (and heads) functional diversity. *Physiology (Bethesda)*. 20:239-251. doi:10.1152/physiol.000142005.

Krause, M., E.W. Dent, J.E. Bear, J.J. Loureiro, and F.B. Gertler. 2003. Ena/VASP proteins: regulators of the actin cytoskeleton and cell migration. *Annu Rev Cell Dev Biol*. 19:541-564. doi:10.1146/annurev.cellbio.19.050103.103356.

Larsson, M., C. Tirado, and S.Wiens. 2017. A Meta-Analysis of Odor Thresholds and Odor Identification in Autism Spectrum Disorders. *Front Psychol*. 8:679. doi: 10.3389/fpsyg.2017.00679.

Laurino, L., X.X. Wang, B.A. de la Houssaye, L. Sosa, S. Dupraz, A. Cáceres, K.H. Pfenninger, and S. Quiroga. 2005. PI3K activation by IGF-1 is essential for the regulation of membrane expansion at the nerve growth cone. J Cell Sci 118:3653–3662. doi:10.1242/jcs.02490.

Lecourtier, L., and P.H. Kelly. 2007. A conductor hidden in the orchestra? Role of the habenular complex in monoamine transmission and cognition. Neurosci Biobehav Rev. 31(5):658–672. doi:10.1016/j.neubiorev.2007.01.004.

Lee, Y.A., and Y. Goto. 2011. Neurodevelopmental disruption of cortico-striatal function caused by degeneration of habenula neurons. PLoS One. 6:e19450. doi:10.1371/journal.pone.0019450.

Lin, Y., J.A. Frei, M.B.C. Kilander, W. Shen, and G.J. Blatt. 2016. A Subset of Autism-Associated Genes Regulate the Structural Stability of Neurons. *Front Cell Neurosci*. 10:263. doi: 10.3389/fncel.2016.00263

Liu, Y.F., S.M. Sowell, Y. Luo, A. Chaubey, R.S. Cameron, H. Kim, and A.K. Srivastava. 2015. Autism and Intellectual Disability-Associated KIRREL3 Interacts with Neuronal Proteins MAP1B and MYO16 with Potential Roles in Neurodevelopment. *PLoS One*. 10(4):e0123106. doi:10.1371/journal.pone.0123106.

Lundmark, R., G.J. Doherty, M.T. Howes, K. Cortese, Y. Vallis, R.G. Parton, and H.T. McMahon. 2008. The GTPase-Activating Protein GRAF1 Regulates the CLIC/CEEC Endocytic Pathway. *Curr Biol.* 18(22):1802-1808. doi:https://doi.org/10.1016/j.cub.2008.10.044.

Manolio, T.A., F.S. Collins, N.J. Cox, D.B. Goldstein, L.A. Hindorff, D.J. Hunter, M.I. McCarthy, E.M. Ramos, L.R. Cardon, A. Chakravarti, J.H. Cho, A.E. Guttmacher, A. Kong, L. Kruglyak, E. Mardis, C.N. Rotimi, M. Slatkin, D. Valle, A.S. Whittemore, M. Boehnke, A.G. Clark, E.E. Eichler, G. Gibson, J.L. Haines, T.F.C. Mackay, S.A. McCarroll, and P.M. Visscher. 2009. Finding the missing heritability of complex diseases. *Nature*. 461:747–753. doi:10.1038/nature08494.

Marin, O. 2012. Interneuron dysfunction in psychiatric disorders. *Nat Rev Neurosci*. 13:107–120. doi:10.1038/nrn3155.

McGann, J.P. 2017. Poor human olfaction is a 19th-century myth. *Science (New York, N.Y.)*. *356*(6338):eaam7263. doi:10.1126/science.aam7263.

Millan, M.J., A. Andrieux, G. Bartzokis, K. Cadenhead, P. Dazzan, P. Fusar-Poli, J. Gallinat, J. Giedd, D.R. Grayson, M. Heinrichs, R. Kahn, M. Krebs, M. Leboyer, D. Lewis, O. Marin, P. Marin, A. Meyer-Lindenberg, P. McGorry, P. McGuire, M.J. Owen, P. Patterson, A. Sawa, M. Spedding, P. Uhlhaas, F. Vaccarino, C. Wahlestedt, and D. Weinberger. 2016. Altering the course of schizophrenia: progress and perspectives. *Nat Rev Drug Discov*. 15(7):485-515 doi:10.1038/nrd.2016.28

Messinger, D., G.S. Young, S. Ozonoff, K. Dobkins, A. Carter, L. Zwaigenbaum, R.J. Landa, T. Charman, W.L. Stone, J.N. Constantino, T. Hutman, L.J. Carver, S. Bryson, J.M. Iverson, M.S. Strauss, S.J. Rogers, and M. Sigman. 2013. Beyond autism: a baby siblings research consortium study of high-risk children at three years of age. *J. Am. Acad. Child Adolesc. Psychiatry* 52:300–308. doi:10.1016/j.jaac.2012.12.011.

Moberg, P.J., V. Kamath, D.M. Marchetto, M.E. Calkins, R.L. Doty, C. Hahn, K.E. Borgmann-Winter, C.G. Kohler, R.E. Gur, and B.I. Turetsky. 2014. Meta-Analysis of Olfactory Function in Schizophrenia, First-Degree Family Members, and Youths At-Risk for Psychosis. 2014. *Schizophr Bull*. 40(1):50–59. doi:10.1093/schbul/sbt049

Moghaddam, B. and D. Javitt. 2012. From revolution to evolution: the glutamate hypothesis of schizophrenia and its implication for treatment. *Neuropsychopharmacology.* 37:4–15. doi:10.1038/npp.2011.181.

Mosavi, L.K., T.J. Cammett, D.C. Desrosiers, and Z.Y. Peng. 2004. The ankyrin repeat as molecular architecture for protein recognition. *Protein Sci*. 13(6):1435-48. doi:10.1110/ps.03554604. PMID: 15152081; PMCID: PMC2279977.

Nagase, T., K. Ishikawa, M. Suyama, R. Kikuno, M. Hirosawa, N. Miyajima, A. Tanaka, H. Kotani, N. Nomura, and O. Ohara. 1998. Prediction of the coding sequences of unidentified human genes. XII. The complete sequences of 100 new cDNA clones from brain which code for large proteins in vitro. *DNA Res.* 5:355–364.

Nakayama, M., R. Kikuno, and O. Ohara. 2002. Protein-protein interactions between large proteins: two-hybrid screening using a functionally classified library composed of long cDNAs. *Genome Res* 12(11):1773–1784. doi:10.1101/ gr.406902.

NCBI Gene: MYO16 myosin XVI [Homo sapiens (human)] [online] Available at: <https://www.ncbi.nlm.nih.gov/gene/23026> [Accessed September 6, 2020].

Nixon, M.A., V. Egger, D.R. Shimshek, R. Renden, I. Fukunaga, R. Sprengel, P.H. Seeburg, M. Klugmann, T.W. Margie, A.T. Schaefer, and T. Kuner. 2010. Synaptic Inhibition in the Olfactory Bulb Accelerates Odor Discrimination in Mice. *Neuron*. 65(3):399-411. doi:10.1016/j.neuron.2010.01.009.

Palumbo, F., B. Serneels, R. Pelagrims, and E. Yaksi. 2020. The Zebrafish Dorsolateral Habenula Is required for Updating Learned Behaviors. *Cell reports.* 32(8):108054. doi:10.1016/j.celrep.2020.108054.

Patel, K.G., C. Liu, P.L. Cameron, and R.S. Cameron. 2001. Myr 8, A Novel Unconventional Myosin Expressed during Brain Development Associates with the Protein Phosphatase Catalytic Subunits 1α and 1γ. *J Neurosci*. 21(20):7954–7968. doi:10.1523/JNEUROSCI.21-20-07954.2001.

Patel, K.R., J. Cherian, K. Gohil, and D. Atkinson. 2014. Schizophrenia: overview and treatment options. *P & T : a peer-reviewed journal for formulary management*, 39(9): 638–645.

Peça, J., and G. Feng. 2012. Cellular and synaptic network defects in autism. *Curr Opin Neurobiol*. 22(5):866-872. doi:10.1016/j.conb.2012.02.015.

Penzes, P., M.E. Cahill, K.A. Jones, J.E. VanLeeuwen, and K.M. Woolfrey. 2011. Dendritic spine pathology in neuropsychiatric disorders. *Nat Neurosci*. 14(3):285-293. doi:10.1038/nn.274.

Pettersson-Yeo, W., P. Allen, S. Benetti, P. McGuire, and A. Mechelli. 2011. Dysconnectivity in schizophrenia: where are we now? *Neurosci Biobehav Rev.* 35:1110–11124. doi:10.1016/j.neubiorev.2010.11.004.

Prehoda, K.E., J.L. Do, and W.A. Lim. 1999. Structure of the Enabled/VASP homology 1 domain-peptide complex: a key component in the spatial control of actin assembly. *Cell*. 97:471–480. doi:10.1016/s0092-8674(00)80757-6.

Rapoport, J.L., J.N. Giedd, and N. Gogtay. 2012. Neurodevelopmental model of schizophrenia: update 2012. *Mol Psychiatry.* 17:1228–1238. doi:10.1038/mp.2012.23.

Roberts, J.L., K. Hovanes, M. Dasouki, A.M. Manzardo, and M.G. Butler. 2014. Chromosomal microarray analysis of consecutive individuals with autism spectrum disorders or learning disability presenting for genetic services. *Gene*. 535 70–78. 10.1016/j.gene.2013.10.020

Rodgers, E.E., and A.B. Theibert. 2002. Functions of PI 3-kinase in development of the nervous system. Int J Dev Neurosci. 20:187–197. doi:10.1016/s0736-5748(02)00047-3.

Rodriguez-Murillo, L., B. Xu, J.L. Roos, G.R. Abecasis, J.A. Gogos, and M. Karayiorgou. 2014. Fine mapping on chromosome 13q32-34 and brain expression analysis implicates MYO16 in schizophrenia. *Neuropsychopharmacology*. 39(4):934-943. doi:10.1038/npp.2013.293.

Roesler, M.K., F.L. Lombino, S. Freitag, M. Schweizer, I. Hermans-Borgmeyer, J.R. Schwarz, M. Kneussel, and W. Wagner. 2019. Myosin XVI Regulates Actin Cytoskeleton Dynamics in Dendritic Spines of Purkinje Cells and Affects Presynaptic Organization. *Front Cell Neurosci*. 13:330. doi:10.3389/fncel.2019.00330.

Rosenblatt, J., L.P. Cramer, B. Baum, and K.M. McGee. 2004. Myosin II-Dependent Cortical Movement Is Required for Centrosome Separation and Positioning during Mitotic Spindle Assembly. Cell. 117(3):361–372. doi:10.1016/S0092-8674(04)00341-1.

Sainath, R., and G. Gallo. 2015. Cytoskeletal and signaling mechanisms of neurite formation. *Cell Tissue Res*. 359(1):267-78. doi:10.1007/s00441-014-1955-0

Samsam, M., R. Ahangari., and S.A. Naser. 2014. Pathophysiology of autism spectrum disorders: revisiting gastrointestinal involvement and immune imbalance. *World J Gastroenterol.* 20(29):9942–9951. doi:10.3748/wjg.v20.i29.9942.

Sanchez, A.D., and J.L. Feldman. 2017. Microtubule-organizing centers: from the centrosome to non-centrosomal sites. *Curr Opin Cell Biol*. *44*:93–101. doi:10.1016/j.ceb.2016.09.003.

Scheuss, V., and T. Bonhoeffer. 2014. Function of Dendritic Spines on Hippocampal Inhibitory Neurons. *Cereb Cortex*. 24(12):3142–3153. doi: 10.1093/cercor/bht171.

Sebé-Pedrós, A., X. Grau-Bové, T. A. Richards, and I. Ruiz-Trillo. 2014. Evolution and classification of myosins, a paneukaryotic whole-genome approach. *Genome Biol. Evol. 6*(2):290–305. doi:10.1093/gbe/evu013.

Sellers, J.R. 2000. Myosins: a diverse superfamily. *Biochim Biophys Acta.* 1496:3-22. doi:10.1016/s0167-4889(00)00005-7.

SFARI database: MYO16 [online] Available at: <https://gene.sfari.org/database/human-gene/MYO16> [Accessed April, 2021].

Soderling, S.H., E.S. Guire, S. Kaech, J. White, F. Zhang, K. Schutz, L.K. Langeberg, G. Banker, J. Raber, and J.D. Scott. 2007. A WAVE-1 and WRP Signalling Complex Regulates Spine

Density, Synaptic Plasticity, and Memory. *J Neurosci*. 27(2):355–365. doi:10.1523/JNEUROSCI.3209-06.2006.

Spence, E.F., D.J. Kanak, B.R. Carlson, and S.H. Soderling. 2016. The Arp2/3 complex is essential for distinct stages of spine synapse maturation, including synapse unsilencing. *J Neurosci.* 36: 9696–9709. doi:10.1523/JNEUROSCI.0876-16.2016.

Su, C., K. Menuz, and J.R. Carlson. 2009. Olfactory Perception: Receptors, Cells, and Circuits. *Cell.* 139(1):45-49. doi: 10.1016/j.cell.2009.09.015.

Svitkina, T. 2018. The Actin Cytoskeleton and Actin-Based Motility. *Cold Spring Harb Perspect Biol*. 13(4). doi:10.1101/cshperspect.a018267.

Sweigert, J.R., T. St John, K.K. Begay, G.E. Davis, J. Munson, E. Shankland, A. Estes, S.R. Dager, and N.M. Kleinhans. 2020. Characterizing Olfactory Function in Children with Autism Spectrum Disorder and Children with Sensory Processing Dysfunction. *Brain Sci*.10(6):362. doi:10.3390/brainsci10060362.

SZDB database: MYO16. [online] Available at: http://www.szdb.org/gene_detail.php [Accessed April, 2021].

Takenawa, T., and S. Suetsugu. 2007. The WASP-WAVE protein network: connecting the membrane to the cytoskeleton. *Nat Rev Mol Cell Biol.* 8:37–48. doi:10.1038/nrm2069.

Telek, E., A. Kengyel, and B. Bugyi. 2020. Myosin XVI in the Nervous System. *Cells.* 9:1903. doi:10.3390/cells9081903.

The Human Protein Atlas: MYO16. [online] Available at: <https://www.proteinatlas.org/ENSG00000041515-MYO16)> [Accessed March, 2021].

Thompson, R.F., and G.M. Langford. 2002. Myosin Superfamily Evolutionary History. *Anat Rec* 268(3):276-289. doi:10.1002/ar.10160.

Tillander V., E. Arvidsson Nordström, J. Reilly, M. Strozyk, P.P. Van Veldhoven, M.C. Hunt, and S.E. 2014. Alexson. Acyl-CoA thioesterase 9 (ACOT9) in mouse may provide a novel link between fatty acid and amino acid metabolism in mitochondria. *Cell Mol Life Sci*. 71(5):933-48. doi:10.1007/s00018-013-1422-1.

Tucker, T., A. Montpetit, D. Chai, S. Chan, S. Chénier, B.P. Coe, A. Delaney, P. Eydoux, W.L. Lam, S. Langlois, E. Lemyre, M. Marra, H. Qian, G.A. Rouleau, D. Vincent, J.L. Michaud, and J.L. Friedman. 2011. Comparison of genome-wide array genomic hybridization platforms for the detection of copy number variants in idiopathic mental retardation. *BMC Med Genet*. *4*:25. doi:https://doi.org/10.1186/1755-8794-4-25.

UniProtKB/Swiss-Prot: MYO16 – Unconventional myosin-XVI. [online] Available at: <https://www.proteinatlas.org/ENSG00000041515-MYO16)> [Accessed March, 2021].

Vijayajumar, N.T., and M.V. Judy. 2015. Autism spectrum disorders: Integration of the genome, transcriptome and the environment. *J Neurol Sci.* 364:167-176. doi:10.1016/j.jns.2016.03.026.

Van den Heuvel, M. P., and A. Fornito. 2014. Brain networks in schizophrenia. *Neuropsychol Rev.* 24:32–48. doi:10.1007/s11065-014-9248-7.

van Kerkhof, L.W., R. Damsteegt, V. Trezza, P. Voorn, and L.J. Vanderschuren. 2013. Functional integrity of the habenula is necessary for social play behaviour in rats. *Eur J Neurosci*. 38(10):3465-3475. doi:10.1111/ejn.12353.

Wagner, W., S.D. Brenowitz, and J.A. Hammer III. 2011. Myosin-Va transports the endoplasmic reticulum into the dendritic spines of Purkinje neurons. *Nat Cell Biol*. 13:40–48. doi:10.1038/ncb2132.

Wang, K., H. Zhang, D. Ma, M. Bucan, J.T. Glessner, B.S. Abrahams, D. Salyakina, M. Imielinski, J.P. Bradfield, P.M. Sleiman, C.E. Kim, C. Hou, E. Frackelton, R. Chiavacci, N. Takahashi, T. Sakurai, E. Rappaport, C.M. Lajonchere, J. Munson, A. Estes, O. Korvatska, J. Piven, L.I. Sonnenblick, A.I. Alvarez Retuerto, E.I. Herman, H. Dong, T. Hutman, M. Sigman, S. Ozonoff, A. Klin, T. Owley, J.A. Sweeney, C.W. Brune, R.M. Cantor, R. Bernier, J.R. Gilbert, M.L. Cuccaro, W.M. McMahon, J. Miller, M.W. State, T.H. Wassink, H. Coon, S.E. Levy, R.T. Schultz, J.I. Nurnberger, J.L. Haines, J.S. Sutcliffe, E.H. Cook, N.J. Minshew, J.D. Buxbaum, G. Dawson, S.F. Grant, D.H. Geschwind, M.A. Pericak-Vance, G.D. Schellenberg, and H. Hakonarson. 2009. Common genetic variants on 5p14.1 associate with autism spectrum disorders. *Nature (London).* 28;459(7246):528-533. doi:10.1038/nature07999.

Wang, Z., J.G. Edwards, N. Riley, D.W. Jr Provance, R. Karcher, X.D.. Li, I.G. Davison, M. Ikebe, J.A. Mercer, J.A. Kauer, and M.D. Ehlers. 2008. Myosin Vb mobilizes recycling endosomes and AMPA receptors for postsynaptic plasticity. *Cell*. 135(3):535-548. doi:10.1016/j.cell.2008.09.057.

Zhao, X., and A. Bhattacharyya. 2018. Human Models Are Needed for Studying Human Neurodevelopmental Disorders. *Am J Hum Genet.* 103(6):829–857. doi:10.1016/j.ajhg.2018.10.009.

Zhao, Z., J. Xu, J. Chen, S. Kim, M. Reimers, S.A. Bacanu, H. Yu, C. Liu, J. Sun, Q. Wang, P. Jia, F. Xu, Y. Zhang, K.S. Kendler, Z. Peng, and X. Chen. 2015. Transcriptome sequencing and genome-wide association analyses reveal lysosomal function and actin cytoskeleton remodeling in schizophrenia and bipolar disorder. *Mol Psy*. 20(5):563–572. doi:10.1038/mp.2014.82.

Zoghbi, H.Y., and M.F. Bear. 2012. Synaptic dysfunction in neurodevelopmental disorders associated with autism and intellectual disabilities. *Cold Spring Harb Perspect Biol.* 4(3):a009886. doi:10.1101/cshperspect.a009886.